Draft version September 25, 2014
Preprint typeset using LaTeX style emulateapj v. 5/2/11

arXiv:1409.6720v1 [astro-ph.GA] 23 Sep 2014

TRACING THE COSMIC METAL EVOLUTION IN THE LOW-REDSHIFT INTERGALACTIC MEDIUM

J. Michael Shull[a], Charles W. Danforth, and Evan M. Tilton
CASA, Department of Astrophysical & Planetary Sciences,
University of Colorado, Boulder, CO 80309, USA
[a]also at Institute of Astronomy, University of Cambridge, Cambridge, CB3 OHA, UK

Draft version September 25, 2014

ABSTRACT

Using the Cosmic Origins Spectrograph aboard the *Hubble Space Telescope*, we measured the abundances of six ions (C III, C IV, Si III, Si IV, N V, O VI) in the low-redshift ($z \leq 0.4$) intergalactic medium (IGM) and explored C and Si ionization corrections from adjacent ion stages. Both C IV and Si IV have increased in abundance by a factor of ~ 10 from $z \approx 5.5$ to the present. We derive ion mass densities, $\rho_{\rm ion} \equiv \Omega_{\rm ion}\rho_{\rm cr}$, with $\Omega_{\rm ion}$ expressed relative to closure density. Our models of the mass-abundance ratios (Si III/Si IV) $= 0.67^{+0.35}_{-0.19}$, (C III/C IV) $= 0.70^{+0.43}_{-0.20}$, and $(\Omega_{\rm CIII} + \Omega_{\rm CIV})/(\Omega_{\rm SiIII} + \Omega_{\rm SiIV}) = 4.9^{+2.2}_{-1.1}$ are consistent with a hydrogen photoionization rate $\Gamma_{\rm H} = (8 \pm 2) \times 10^{-14}$ s^{-1} at $z < 0.4$ and specific intensity $I_0 = (3 \pm 1) \times 10^{-23}$ erg cm^{-2} s^{-1} Hz^{-1} sr^{-1} at the Lyman limit. We find mean photoionization parameter $\log U = -1.5 \pm 0.4$, baryon overdensity $\Delta_b \approx 200 \pm 50$, and Si/C enhanced to three times its solar ratio (enhancement of alpha-process elements). We compare these metal abundances to the expected IGM enrichment and abundances in higher photoionized states of carbon (C V) and silicon (Si V, Si VI, Si VII). Our ionization modeling infers IGM metal densities of $(5.4 \pm 0.5) \times 10^5\ M_\odot$ Mpc^{-3} in the photoionized Lyα forest traced by the C and Si ions and $(9.1 \pm 0.6) \times 10^5\ M_\odot$ Mpc^{-3} in hotter gas traced by O VI. Combining both phases, the heavy elements in the IGM have mass density $\rho_Z = (1.5 \pm 0.8) \times 10^6\ M_\odot$ Mpc^{-3} or $\Omega_Z \approx 10^{-5}$. This represents $10 \pm 5\%$ of the metals produced by $(6 \pm 2) \times 10^8\ M_\odot$ Mpc^{-3} of integrated star formation with yield $y_m = 0.025 \pm 0.010$. The missing metals at low redshift may reside within galaxies and in undetected ionized gas in galaxy halos and circumgalactic medium.

1. INTRODUCTION

It is still uncertain whether a "missing metals" problem exists for galaxies and the intergalactic medium (IGM). The problem was originally proposed (Pettini 1999) as a mismatch between the expected production rate of heavy elements (metals) and the observed metallicities in galaxies and quasar absorption-line systems. The metal production rate, $\dot{\rho}_Z = y_m \dot{\rho}_*$, can be related to $\dot{\rho}_*$, the star formation rate (SFR) density, times the metal yield y_m, estimated to lie in the range 0.016-0.048 depending on the stellar initial mass function (IMF) and nucleosynthetic yields of massive stars and supernovae (Madau & Dickinson 2014). The majority of the heavy elements produced by star formation in the last 10-13 Gyr were undetected in damped Lyα absorbers (DLAs; Wolfe et al. 2003) or Lyman-break galaxies (LBGs, Steidel et al. 1999). Several solutions were proposed for this missing-metals problem, including the possibility that heavy elements are stored in gaseous halos or expelled to the IGM by galaxy winds (Ferrara et al. 2005; Bouché et al. 2007) or into the circumgalactic medium (CGM) as suggested by Tumlinson et al. (2011).

Early tests of the IGM hypothesis measured the metallicity at redshifts $z \approx 2-4$ (Songaila 2001, 2005; Pettini et al. 2003; Boksenberg et al. 2003; Schaye et al. 2003; Aguirre et al. 2004) using quasar absorption lines of C IV ($\lambda\lambda 1548, 1551$) and Si IV ($\lambda\lambda 1393, 1403$). These rest-frame ultraviolet (UV) lines are observable with ground-based telescopes for absorption systems that shift into the optical band at $z > 1.5$. Shorter-wavelength transitions of O VI ($\lambda\lambda 1032, 1038$), Si III ($\lambda 1206$), and C III ($\lambda 977$) are shifted into the optical at higher redshifts, but confusion with the strong Lyα forest complicates their measurement. Metal absorption-line studies have now been extended to larger redshifts $z \approx 5-6$ (Simcoe 2006, 2011; Becker et al. 2009; Ryan-Weber et al. 2006, 2009) with three recent studies (Simcoe et al. 2011; D'Odorico et al. 2013; Cooksey et al. 2013) superseding prior work at high redshift. At $z < 1.5$, most diagnostic absorption lines fall in the ultraviolet and require observations from space with the *Hubble Space Telescope* (*HST*) and *Far Ultraviolet Spectroscopic Explorer* (Penton et al. 2000, 2004; Danforth & Shull 2005, 2008; Cooksey et al. 2010).

In this paper, we analyze the metal-line results obtained from our recent survey of the low-redshift IGM with the Cosmic Origins Spectrograph (COS) on *HST* (Danforth et al. 2014). Observing at low redshifts avoids the complications of the Lyα forest, probes the absorbers directly in the rest-frame UV, and provides access to a wider range of ionization states. The current COS survey provides the largest sample of low-z IGM absorbers to date, with a total redshift pathlength $\Delta z \approx 20$ in H I. In Section 2 we describe the portion of the survey relevant to the column density distributions and mass densities of six metal ions, for which we have accumulated a substantial number of absorbers. Our results are described in Section 3, where we derive low-z mass densities, $\Omega_{\rm ion}$, for all six ions. The availability of data from adjacent ionization states of the same element (C III, C IV and Si III, Si IV) allows us to estimate photoionization conditions and correct for unseen ion states. Because line-blanketing by the Lyα forest is generally not a problem ($< 2\%$ at low redshifts) these abundances provide accurate values of nucleosynthetically interesting abundance ratios (O/C, O/N, Si/C). In Section 4, we summarize the low-z metallicity and its relevance to SFR history, and we assess whether a missing-metals issue still exists.

michael.shull@colorado.edu, danforth@colorado.edu, evan.tilton@colorado.edu

2. OBSERVATIONAL DATA

We have observed six ions (C III, C IV, N V, O VI, Si III Si IV) in the low-redshift IGM, using the *HST* Cosmic Origins Spectrograph (Green et al. 2012) in the medium-resolution mode ($R \approx 18,000$, $\Delta v \approx 17$ km s^{-1}) with the G130M and G160M gratings that cover 1135–1796 Å. Complete results of our IGM survey in the far-UV are given in Danforth et al. (2014), a study of 75 AGN sight lines that detected over 2500 H I absorption systems accompanied by more than 350 metal-line systems. Table 1 provides details on the ions, the number of metal-ion absorbers, their atomic data, and the accessible redshift ranges covered by the G130M and G160M gratings.

To obtain gas-phase IGM metal abundances, we follow the standard technique of measuring absorption lines of the UV resonance transitions of key ion species and making ionization corrections. Most metallicity surveys are made with one or both lines of the doublet transitions of C IV (*2s-2p* 1548.204, 1550.781 Å) and Si IV (*3s-3p* 1393.760, 1402.773 Å) owing to their line strength and accessibility longward of the Lyα forest ($\lambda_{\rm rest} > 1215.67$ Å). Although line-blanketing by the Lyα forest becomes strong at high redshift, our COS survey has access to the doublet transition of O VI (*2s-2p* 1031.926, 1037.617 Å) and single-line absorption from strong transitions of C III (*2s*^{2}*-2s 2p* 977.020 Å) and Si III (*3s*^{2}*-3s 3p* 1206.500 Å). This list is supplemented by the N V doublet (*2s-2p* 1238.82, 1242.804 Å). The C III and C IV absorbers are not present in the same gas, since C III λ977 shifts into the G130M band at $z > 0.162$ and C IV λ1548 shifts out of the G160M band at $z > 0.160$. Thus, the ion-ratio comparisons with COS data are statistical. We have also examined the C III/ C IV ratio in our STIS + FUSE survey (Tilton et al. 2012) where both lines are present in the same absorbers; we find good agreement with the COS results.

3. RESULTS AND INTERPRETATION

3.1. *Metal Ion Abundances in the IGM*

We express the mass density of a metal ion, $\rho_{\rm ion} = \Omega_{\rm ion}\rho_{\rm cr}$, relative to $\rho_{\rm cr}$, the cosmological closure density. For Hubble constant $H_0 = (70$ km s^{-1} Mpc$^{-1})h_{70}$, we can write $\rho_{\rm cr} = (3H_0^2/8\pi G) = 9.205 \times 10^{-30}\ h_{70}^2$ g cm^{-3}, or in more convenient galactic units, $1.36 \times 10^{11}\ h_{70}^2\, M_\odot$ Mpc^{-3}. The mean comoving baryon overdensity (at $z = 0$) is written $\bar{\rho}_b = [\Omega_b \rho_{\rm cr}(1 - Y_p)/m_H] \approx 1.90 \times 10^{-7}$ cm^{-3}, appropriate for $\Omega_b = 0.0461$ (Hinshaw et al. 2013) and primordial helium abundance $Y_p = 0.2485$ (Aver et al. 2013). The ion mass density is found by integrating over its observed column density distribution function (CDDF) of absorbers, $f(N,z) \equiv (\partial^2\mathcal{N}/\partial N\,\partial z)$, as described in Tilton et al. (2012),

$$\Omega_{\rm ion} = \frac{H_0\, m_{\rm ion}}{c\,\rho_{\rm cr}} \int_{\rm N_{min}}^{\rm N_{max}} f(N,z)\, N\, dN$$
$$= (1.365 \times 10^{23}\ {\rm cm}^2)\, h_{70}^{-1} \left(\frac{m_{\rm ion}}{\rm amu}\right) \int_{\rm N_{min}}^{\rm N_{max}} f(N,z)\, N\, dN \quad (1)$$

The integral is performed as a sum over logarithmic bins of size $\Delta \log N \approx 0.2$. The range of integration is set at the lower end ($N_{\rm min}$) by our 30 mÅ equivalent width threshold and at the upper end ($N_{\rm max}$) by the column density where absorber statistics become uncertain. Depending on the slope of the distribution, $f(N,z) \propto N^{-\beta}$, we can make corrections for absorption systems outside this range. Appendix A describes our formalism for fitting these distributions and integrating power-law fits to $f(N,z)$. This technique provides a check on the numerical integration and allows us to assess the fiducial metal content, extrapolated to column densities above and below the observed range.

Table 2 gives the $\Omega_{\rm ion}$ values for all six ions, measured in low-z surveys with HST/STIS (Tilton et al. 2012) and HST/COS (Danforth et al. 2014). Although our metal absorber list is large, there is considerable overlap with prior studies (Danforth & Shull 2008; Cooksey et al. 2011; Tilton et al. 2012). We express values of $\Omega_{\rm ion}$ in units of $10^{-8}h_{70}^{-1}$. All values from our previous STIS survey were recalculated from the Tilton et al. (2012) absorber lists to match the column density ranges in Table 2. We then compare the low-z measurements to values from previous surveys, including Songaila (2001, 2005), Becker et al. (2009), Simcoe (2006), Simcoe et al. (2011), and Ryan-Weber et al. (2006). All values of $\Omega_{\rm ion}$ were revised to agree with our adopted (ΛCDM) cosmological parameters, $h = 0.7$, $\Omega_m = 0.275$, $\Omega_\Lambda = 0.725$.

The distributions in column density were shown in Danforth et al. (2014) plotted versus column density, $N_{\rm ion}$, for C IV, Si IV, C III, Si III, and O VI. These distributions illustrate the systematic uncertainties inherent in computing values of $\Omega_{\rm ion}$ from Equation (1) over the measured range of column densities ($\log N_{\rm min} < \log N < \log N_{\rm max}$). For several ions, the discrete sums are sensitive to the small number of absorbers at the high end, as well as the reduced pathlength Δz for absorbers at the low end. As was done by previous authors (Cooksey et al. 2010, 2013; D'Odorico et al. 2013) we fit power laws to the CDDF and extrapolate to a standard range of column densities as discussed in Appendix A and Table 3. These distributions are often more useful to observers than the single parameter $\Omega_{\rm ion}$, and they convey information about the sparse statistics for metal absorbers at both low and high column densities.

Figure 1 shows the evolution of $\Omega_{\rm CIV}$ with redshift. The C IV data include high-redshift measurements ($z \approx 4.5 - 6$) by Pettini et al. (2003), Becker et al. (2009), Ryan-Weber et al. (2009), Simcoe et al. 2011), and D'Odorico et al. (2013). We corrected the Pettini results for our values of H_0 and Ω_m using the scaling $\Omega_{\rm ion} \propto \Omega_m^{1/2} h^{-1}$. Values at intermediate redshifts ($z \approx 1.6 - 4.5$) are taken from surveys by Boksenberg et al. (2003), D'Odorico et al. (2010), and Boksenberg & Sargent (2014). The latter paper includes updated values for $\Omega_{\rm CIV}$ provided by A. Boksenberg (2014, private communication). The data at $z < 1$ come from the HST survey by Cooksey et al. (2010) reported in two

redshift bins: $\Omega_{\rm CIV} = 6.24^{+2.88}_{-2.14}$ $(10^{-8}h_{70}^{-1})$ from 17 C IV absorbers at $\langle z\rangle = 0.383$ and $\Omega_{\rm CIV} = 6.35^{+2.52}_{-1.99}(10^{-8}h_{70}^{-1})$ from 19 C IV absorbers at $\langle z\rangle = 0.786$. For the entire redshift sample, they found $\Omega_{\rm CIV} = 6.20^{+1.82}_{-1.52}$ $(10^{-8}h_{70}^{-1})$ from 36 C IV absorbers at $\langle z\rangle = 0.654$. The lowest redshift points at $\langle z\rangle < 0.1$ come from the Colorado group's surveys: $\Omega_{\rm CIV} = 7.7 \pm 1.5$ $(10^{-8}h_{70}^{-1})$ from 24 C IV absorbers (Danforth & Shull 2008), $\Omega_{\rm CIV} = 8.1^{+4.6}_{-1.7}$ $(10^{-8}h_{70}^{-1})$ from 29 C IV absorbers (Tilton et al. 2012), and $\Omega_{\rm CIV} = 10.1^{+5.6}_{-2.4}$ $(10^{-8}h_{70}^{-1})$ from 49 C IV absorbers (Danforth et al. 2014).

Figure 2 shows the evolution of $\Omega_{\rm SiIV}$ with redshift, including high-redshift measurements ($z \approx 2-5$) by Songaila (2001, 2005) converted to our parameters (H_0 and Ω_m). We also show data at $z \approx 2.4$ (Scannapieco et al. 2006), at $z \approx 3.3$ (Aguirre et al. 2004), and at $z = 1.9-4.5$ (Boksenberg & Sargent 2014). The latter paper includes new values for $\Omega_{\rm SiIV}$ provided by A. Boksenberg (2014, private communication.) The low-redshift data come from the HST survey by Cooksey et al. (2011) at $z < 1$. The lowest redshift points at $\langle z\rangle < 0.1$ are based on the Colorado group's recent surveys: $\Omega_{\rm SiIV} = 4.5^{+3.0}_{-1.2}$ $(10^{-8}h_{70}^{-1})$ from 30 Si IV absorbers (Tilton et al. 2012) and $\Omega_{\rm SiIV} = 2.1^{+1.0}_{-0.5}$ $(10^{-8}h_{70}^{-1})$ from 31 Si IV absorbers (Danforth et al. 2014). Evidently, the Si IV measurements still have some uncertainty arising from the column density distribution function.

3.2. *Metagalactic Ionizing Background*

In Section 3.3 we will analyze the ionization states of C, Si, and O probed by the observed ions. This analysis requires photoionization modeling using estimates of the metagalactic flux of ionizing photons. Through analytic formulae, we can relate the hydrogen photoionization rate $\Gamma_{\rm H}$ for optically thin absorbers to the specific intensity I_ν and its value I_0 at the Lyman limit (912 Å), as well as to Φ_0, the one-sided (unidirectional) flux of ionizing photons. Because there has been some debate in the modeling literature over the strength of the metagalactic ionizing radiation field, we begin with clear definitions of flux and intensity. Part of the confusion arises from geometric differences between an isotropic radiation field, appropriate for intergalactic space far from individual sources, and a unidirectional radiation field arising from a single nearby source. In models for the local-source case, all photons enter the absorber at normal incidence from one side. In the isotropic case, half the photons are directed into the forward hemisphere and half backward. One must also account for the angular dependence of the radiation, with $\langle\cos\theta\rangle = 1/2$ averaged over the forward hemisphere. Thus, for an isotropic radiation field, the unidirectional flux $\Phi_0 = n_\gamma(c/4)$, and for the local source $\Phi_0 = n_\gamma c$, where n_γ is the number density of ionizing photons. Geometric factors are less critical for optically thin absorber models, but one must be careful when using flux or intensity parameters to derive n_γ, the photoionization parameter $U = n_\gamma/n_{\rm H}$, and the ionization fractions of H, He, and heavy elements.

The ionizing radiation background remains somewhat uncertain, despite two decades of estimating its strength and spectrum (Haardt & Madau 1996, 2001, 2012; Shull et al. 1999; Faucher-Giguère et al. 2009). Figure 3 shows several estimates of the ionizing background in the extreme ultraviolet (EUV) and soft X-ray. The labels (HM01, HM05, HM12, FG11) refer to published or unpublished tabulations based on earlier publications. The HM05 spectrum refers to the 2005 August update to the Haardt & Madau (2001) radiation field[1] and the FG11 spectrum refers to the 2011 December update[2] to the spectrum in Faucher-Giguère et al. (2009). The PL spectrum refers to our constructed broken power-law distribution consistent with recent *HST*/COS composite spectrum (Shull et al. 2012) in the EUV (500-912 Å) and connected to soft X-ray observations in the Lockman Hole (Hasinger 1994). The hard X-ray background (Churazov et al. 2007) from 10–100 keV has been included in some backgrounds (HM01, HM05, HM12); these energetic photons have little effect on the ionization state of H, He, and heavy elements.

The hydrogen-ionizing background Φ_0 and photoionization rate $\Gamma_{\rm H}$ of HM12 have been questioned (Kollmeier et al. 2014) as inconsistent with the column density distribution of low-redshift Lyα (H I) absorbers (Danforth et al. 2014). The numerical simulations in their analysis were based on the HM12 background, which was deemed too low by a factor of 5. However, they noted better agreement when the HM01 background was used. A similar comparison (Egan et al. 2014) also obtained good agreement with the Lyα distribution, using our group's grid-code (`Enzo`) simulations (Smith et al. 2011) based on the HM01 ionizing background. The primary difference between HM01 and HM12 radiation fields comes from different assumptions about the escape fraction ($f_{\rm esc}$) of Lyman continuum (LyC) radiation from galaxies (Shull et al. 1999). In the HM12 formulation, the ionizing background is dominated by AGN, the escape fraction is parameterized as $f_{\rm esc}(z) \approx (1.8\times10^{-4})(1+z)^{3.4}$, and galaxies make essentially no contribution to the photoionization rate at $z < 1$. Such low values of $f_{\rm esc}$ are probably unrealistic, since the usual observational constraints (direct LyC detection, diffuse Hα emission, and metal ion ratios) depend on small-number statistics and geometric uncertainties. If the LyC photons escape through vertical cones above star-forming regions in galactic disks (Dove & Shull 1994), the observational constraints require large samples to deal with inclination bias. High-redshift surveys (Shapley et al. 2006) find either large transmitted LyC fluxes or none at all. As a consequence, if $f_{\rm esc}$ were only 5%, one would need to survey well over 20 galaxies to obtain a statistically accurate escape fraction.

Systematic uncertainties also affect indirect limits on the metagalactic background from diffuse Hα emission (Stocke et al. 1991; Donahue et al. 1995; Vogel et al. 1995; Weymann et al. 2001). Translating Hα surface brightnesses into limits on Φ_0 or $\Gamma_{\rm H}$ requires assumptions about emitting geometries and radiative transfer of LyC. Adams et al. (2011) used integral-field spectroscopy to set deep limits on Hα emission from the outskirts of two low surface brightness, edge-on Sd

[1] Unpublished version of the metagalactic Quasars+Galaxies ionizing spectra described in Haardt & Madau (2001) and provided for inclusion in CLOUDY.

[2] Retrieved from `http://galaxies.northwestern.edu/uvb/`

galaxies, UGC 7321 and UGC 1281. They constrained the H I photoionization rate to be $\Gamma_{\rm H} < 2.3 \times 10^{-14}$ s^{-1} (UGC 7321) and $\Gamma_{\rm H} < 14 \times 10^{-14}$ s^{-1} (UGC 1281). The UGC 7321 limit comes from a (5σ) absence of Hα, and it lies well below previous observational limits and theoretical predictions. However, we are reluctant to adopt such a low value of $\Gamma_{\rm H}$ or Φ_0 from a single object[3]. Their method of inferring the metagalactic flux Φ_0 and ionization rate $\Gamma_{\rm H}$ relies on a large and uncertain geometric correction for the gas cloud aspect ratio, $A_{\rm tot}/A_{\rm proj}$, of total exposed area to projected area. As noted by Stocke et al. (2001), this ratio is 4 for a sphere and π for a cylinder viewed transversely. The value $\langle A_{\rm tot}/A_{\rm proj}\rangle = 24.8^{+3.4}_{-1.5}$ adopted by Adams et al. (2011) is based on the projection of a homogeneous thin disk viewed nearly edge-on, whereas the Hα emission likely arises in smaller clumps of gas, whose geometries are probably closer to spheres or cylinders. With the inferred ionizing flux scaling as $\Phi_0 \propto (A_{\rm tot}/A_{\rm proj})^{-1}$, their lower limit arises from a 6-8 times larger aspect ratio compared to values for spherical or cylindrical clouds.

In view of the extensive experimental and theoretical literature on metagalactic fluxes, hydrogen ionization rates, and IGM ionization conditions, the limits on low-redshift ionizing radiation remain uncertain. In Section 3.3, we use ratios of adjacent ion stages (C III/C IV and Si III/Si IV) from IGM absorption-line spectroscopy to constrain $\Phi_0 \approx 10^4$ cm^{-2} s^{-1}. A similar technique, based on the ions Fe I/Fe II and Mg I/Mg II in the low-redshift absorption system around NGC 3067 probed by the background QSO 3C 232, gave a lower limit $\Phi_0 > 2600$ cm^{-2} s^{-1}. Our models in Section 3.3 use $\Phi_0 \approx 10^4$ cm^{-2} s^{-1}, $\Gamma_{\rm H} \approx (8 \pm 2) \times 10^{-14}$ s^{-1}, and $I_0 \approx (3 \pm 1) \times 10^{-23}$ erg cm^{-2} s^{-1} Hz^{-1} sr^{-1}. These parameters are in reasonable agreement with past calculations, observational estimates (other than the single galaxy probed by Adams et al. 2011), and with our low-redshift absorber data on C III, C IV, Si III, and Si IV. We now explore this issue quantitatively.

For an isotropic radiation field of specific intensity I_ν, the normally incident photon flux per frequency is $(\pi I_\nu/h\nu)$ into an angle-averaged, forward-directed effective solid angle of π steradians. The isotropic photon flux striking an atom or ion is $4\pi(I_\nu/h\nu)$. The hydrogen photoionization rate follows by integrating this photon flux times the photoionization cross section over frequency from threshold (ν_0) to ∞.

$$\Gamma_{\rm H} = \int_{\nu_0}^{\infty} \frac{4\pi\, I_\nu}{h\nu} \sigma_\nu \, d\nu \approx \left(\frac{4\pi I_0 \sigma_0}{h}\right) \int_1^\infty x^{-\alpha-\beta-1}\, dx = \frac{4\pi I_0 \sigma_0}{h(\alpha+\beta)} \; . \quad (2)$$

Here, we define the dimensionless variable $x = \nu/\nu_0$ and approximate the frequency dependence of specific intensity and photoionization cross section by power laws, $I_\nu = I_0(\nu/\nu_0)^{-\alpha}$ and $\sigma_\nu = \sigma_0(\nu/\nu_0)^{-\beta}$, where $\sigma_0 = 6.30 \times 10^{-18}$ cm^2 and $\beta \approx 3$. The integrated unidirectional flux of ionizing photons is

$$\Phi_0 = \int_{\nu_0}^{\infty} \frac{\pi I_\nu}{h\nu}\, d\nu = \left(\frac{\pi I_0}{h}\right) \int_1^\infty x^{-\alpha-1}\, dx = \frac{\pi I_0}{h\alpha} \; , \quad (3)$$

which can be related to the density of hydrogen-ionizing photons by $\Phi_0 = n_\gamma(c/4)$. We note that this definition differs by a factor of 1/4 from that in Cloudy, which adopts the convention that $\Phi_0 = n_\gamma c$, appropriate for all photons arriving at normal incidence from one direction. We then use $I_0 = (h\alpha/\pi)\Phi_0$ to relate $\Gamma_{\rm H}$ to the flux and spectrum parameters:

$$\Gamma_{\rm H} = 4\sigma_0\Phi_0 \left(\frac{\alpha}{\alpha+\beta}\right) = (8.06 \times 10^{-14}\ {\rm s}^{-1})\Phi_4 \quad (4)$$

$$\Gamma_{\rm H} = \left(\frac{4\pi I_0 \sigma_0}{\alpha+\beta}\right) = (2.71 \times 10^{-14}\ {\rm s}^{-1}) I_{-23} \; . \quad (5)$$

We will see that $\Phi_4 \approx 1$ and $I_{-23} \approx 3$ give reasonable fits to the ionization ratios, where we scale the incident flux of ionizing photons and specific intensity to characteristic values, $\Phi_0 = (10^4\ {\rm cm}^{-2}\,{\rm s}^{-1})\Phi_4$ and $I_0 = (10^{-23}$ erg cm^{-2} s^{-1} Hz^{-1} sr^{-1})I_{-23} at the hydrogen Lyman limit ($h\nu_0 = 13.60$ eV). We adopt $\beta \approx 3$ for hydrogen and an AGN composite spectrum (Shull et al. 2012) with mean spectral index $\alpha \approx 1.41$ between $1.0 - 1.5$ ryd. For these parameters, we can write the photoionization parameter $U = n_\gamma/n_H$ as,

$$U \equiv \left(\frac{4\Phi_0}{n_H c}\right) = (7.02 \times 10^{-2})\Phi_4 \Delta_{100}^{-1} \; , \quad (6)$$

where the absorber hydrogen density is $n_H = (1.90 \times 10^{-7}\ {\rm cm}^{-3})\Delta_b$ at $z = 0$ with baryon overdensity scaled to $\Delta_b \equiv 100\Delta_{100}$.

Recent calculations of the metagalactic ionizing background (Haardt & Madau 2012) yield a hydrogen photoionization rate, which can be fitted to $\Gamma_H = (2.28 \times 10^{-14}\ {\rm s}^{-1})(1+z)^{4.4}$ over the range $0 \le z \le 0.7$. This HM12 ionization rate at $z = 0$ would correspond to $\Phi_0 = [\Gamma_{\rm H}(\alpha+\beta)/4\sigma_0\,\alpha] \approx 2630$ cm^{-2} s^{-1} and $I_{-23} \approx 0.823$ for the radio-quiet AGN spectral index ($\alpha = 1.57$) assumed by HM12. These fluxes are lower by a factor of 3 compared to the $z = 0$ metagalactic radiation fields from AGN and galaxies calculated by Shull et al. (1999), $I_{\rm AGN} = 1.3^{+0.8}_{-0.5} \times 10^{-23}$ and $I_{\rm Gal} = 1.1^{+1.5}_{-0.7} \times 10^{-23}$, respectively. Adding these two values with propagated errors gives a total intensity and hydrogen ionization rate of $I_{\rm tot} = 2.4^{+1.7}_{-0.9} \times 10^{-23}$ erg cm^{-2} s^{-1} Hz^{-1} sr^{-1} and $\Gamma_{\rm H} = 6.0^{+4.2}_{-2.1} \times 10^{-14}$ s^{-1}. These backgrounds are consistent with those that we estimate below from the C and Si ionization states. The difference between these radiation fields appears to be the small contribution of galaxies assumed in the HM12 background compared to that of Shull et al. (1999), HM01, and HM05. For these reasons, as well as the issues raised by Kollmeier et al. (2014), we normalize our modeled spectral energy distributions (SEDs) to unidirectional, normally incident fluxes $\Phi_0 = 10^4$ cm^{-2} s^{-1}, corresponding to specific intensity $I_0 \approx 3 \times 10^{-23}$ erg cm^{-2} s^{-1} Hz^{-1} sr^{-1} and hydrogen photoionization rate $\Gamma_{\rm H} \approx 8 \times 10^{-14}$ s^{-1}.

[3] Their stringent limit comes from UGC 7321, whereas the limit toward UGC 1281 is a factor of 6 higher. In a subsequent AAS abstract (Uson et al. 2012) the same authors claim to have detected Hα emission toward UGC 7321, with an inferred $\Gamma_H = 3.4 \times 10^{-14}$ s^{-1} that is larger than their 2011 upper limit.

3.3. *Metal Densities at Low Redshift*

The IGM metal density traced by these six ion species can be estimated by correcting for unseen ionization states and scaling to total metal abundances. For the latter, we initially adopted solar abundances to compute the fractional contributions of C, Si, or O to the total metal abundances by mass. However, after comparing the C and Si abundances, we prefer an abundance pattern in which alpha-process elements (e.g., Si and O) are enhanced relative to C owing to early nucleosynthesis sources by massive stars. In high-redshift spectra, observers usually measure C IV and Si IV, and sometimes C II and Si II, but they often lack the important intermediate ion states C III and Si III, whose absorption lines at 977.0 Å and 1206.5 Å can be confused by the Lyα forest. Here, in our low-z survey, we measure C III and C IV as well as Si III and Si IV. We use the mean (statistical) values of the ratios of adjacent ion states, C III/C IV and Si III/Si IV, to constrain the IGM density and the strength and shape of the ionizing radiation background. We then use the ionization corrections for C and Si to estimate consistent individual metallicities. By comparing these metallicities to their expected abundance ratios, we derive additional constraints on Si/C abundance enhancement, radiation field, and IGM density.

The mean observed ionization fractions of the ensemble of metal-line absorbers are:

$$\frac{\Omega_{\rm CIII}}{\Omega_{\rm CIV}} = 0.70^{+0.43}_{-0.20} \quad \text{and} \quad \frac{\Omega_{\rm SiIII}}{\Omega_{\rm SiIV}} = 0.67^{+0.35}_{-0.19} \ . \qquad (7)$$

We will show that for a range of ionizing background shapes, these ratios are consistent with photoionization parameter $\log U \approx -1.5 \pm 0.4$. As noted earlier, $U = n_\gamma/n_{\rm H}$ expresses the density ratio of ionizing photons to hydrogen, where $n_{\rm H} = (1.90 \times 10^{-7}\ {\rm cm}^{-3})\Delta_b(1+z)^3$, with baryon overdensity Δ_b. Because the absorption lines of C III λ977 and C IV λ1548 redshift in and out of the COS G130M and G160M bands at $z \approx 0.16$, our COS survey does not observe C III and C IV in the same absorbers. Thus, there may be some concern that these ions are experiencing different radiation fields, in which the ionization parameter, $U(z) \propto (1+z)^{1.4}$ for an ionization rate $\Gamma_{\rm H} \propto (1+z)^{4.4}$ and hydrogen density $n_{\rm H} \propto (1+z)^3$. In the COS sample (Danforth et al. 2014) the mean redshifts of the carbon absorbers are $\langle z_{\rm CIII}\rangle = 0.35$ and $\langle z_{\rm CIV}\rangle = 0.06$, so we might expect a 0.15 dex offset in U between those absorbers. However, we have also examined low-redshift data from our *FUSE* and STIS survey (Tilton et al. 2012), in which both ions are both seen in the same absorbers. In those 28 absorbers, with $\langle z_{\rm CIII}\rangle = 0.15$ and $\langle z_{\rm CIV}\rangle = 0.056$, the C III/C IV ratios are essentially the same as in the COS data. Therefore, we choose to make no correction for possible small offsets in the radiation field.

We explore the ionizing spectra and their effects on the observed ion densities through a series of photoionization calculations with version 13.03 of Cloudy, last described by Ferland et al. (2013). All spectra were flux-normalized to $\Phi_0 = 10^4\ {\rm cm}^{-2}\,{\rm s}^{-1}$. The hydrogen density was related to baryon overdensity Δ_b, and the metallicity in the simulations was taken as 0.1 solar, consistent with inferences for the mean in the low-z IGM (Shull et al. 2012). The input spectra consisted of a variety of SEDs of ionizing photons, reflecting the uncertain intensities in the EUV and soft X-ray (Shull et al. 2012; Haardt & Madau 2012; Faucher-Giguère et al. 2009). We constrain the SED from the observed abundance ratios of adjacent ionization states, C III/C IV and Si III/Si IV and then estimate the total mass densities of C and Si,

$$\Omega_{\rm C} = (\Omega_{\rm CIII} + \Omega_{\rm CIV}) \left(\frac{\rm C_{tot}}{\rm C\ III + C\ IV} \right) \qquad (8)$$

$$\Omega_{\rm Si} = (\Omega_{\rm SiIII} + \Omega_{\rm SiIV}) \left(\frac{\rm Si_{tot}}{\rm Si\ III + Si\ IV} \right) \ . \qquad (9)$$

The second parenthetical terms in these relations are the ionization correction factors, abbreviated ${\rm CF_C}$ and ${\rm CF_{Si}}$, which quantify the amount of C and Si in higher ion states. As discussed more fully in Appendix B, ionizing EUV photons can produce helium-like carbon (C V) by ionizing C IV at energies $E \geq 64.49$ eV. The EUV photons also make Si V, Si VI, Si VII with production threshold energies 33.49 eV (from Si III), 45.14 eV (from Si IV), and 166.77 eV (from Si V) respectively. These ions can also be produced by inner-shell ionization by soft X-rays ($E \geq 1.9$ keV) followed by Auger electron emission, which boosts the ionization by two or more stages. Further discussion and analytic estimates of the abundances of higher ion states of C and Si are provided in Appendix B.

Figure 4 shows the ratios, C III/C IV and Si III/Si IV, as functions of Δ_b, and Figure 5 shows the ionization correction factors ${\rm CF_C}$ and ${\rm CF_{Si}}$ vs. Δ_b for various SEDs. Our Cloudy photoionization models of the observed C and Si ion ratios, together with their uncertainties, suggest that $\Delta_b \approx 70 - 230$ for the HM12 and PL spectral distributions. The agreement is not as good with the FG11 and HM05 background, with HM12 and PL models providing better agreement. The corresponding correction factors to the two observed stages of C and Si are ${\rm CF_C} = \Omega_{\rm C}/\left[\Omega_{\rm CIII} + \Omega_{\rm CIV}\right] = 2.0^{+1.0}_{-0.5}$ and ${\rm CF_{Si}} = \Omega_{\rm Si}/\left[\Omega_{\rm SiIII} + \Omega_{\rm SiIV}\right] = 6^{+4}_{-3}$.

An additional constraint comes from the C and Si metallicities inferred from our ionization corrections, which must be consistent with their relative abundances by mass. For solar abundances, the Si/C ratio is $\rho_{\rm Si}/\rho_{\rm C} = 0.238$ by mass, but our survey suggests that Si must be enhanced by a factor of 3 (Figure 6) probably owing to "alpha-process" nucleosynthesis. Using the observed mass densities in Table 2, $(\Omega_{\rm CIII} + \Omega_{\rm CIV}) = 17.2^{+5.9}_{-2.7}$ $(10^{-8}h_{70}^{-1})$ and $(\Omega_{\rm SiIII} + \Omega_{\rm SiIV}) = 3.5^{+1.0}_{-0.5}$ $(10^{-8}h_{70}^{-1})$, we can relate the Si/C abundance ratio to the ion correction factors:

$$\frac{\rm CF_{Si}}{\rm CF_C} = (1.17^{+0.52}_{-0.25}) \left[\frac{\rho_{\rm Si}/\rho_{\rm C}}{0.238} \right] \ . \qquad (10)$$

From the constraints in Figures 4, 5, and 6, we find that $\Delta_b \approx 200 \pm 50$ for ionizing flux $\Phi_0 = 10^4\ {\rm cm}^{-2}\ {\rm s}^{-1}$. If we were to lower the ionizing background to $\Phi_0 = (3000 - 5000)\ {\rm cm}^{-2}\ {\rm s}^{-1}$, our ionization models for the C and Si ion ratios would require lowering the baryon overdensity to $\Delta_b = 50 - 100$. As can be seen in Figures 4 and 5, the ionization correction factors would then become unrealistically large, particularly for silicon which would rise to ${\rm Si_{tot}}/({\rm Si\ III + Si\ IV}) > 100$. Thus, the observed metal-line systems probably reside in higher

density regions than Lyα-forest systems at lower column densities. Therefore, the observed ionization ratios of C III/C IV and Si III/Si IV provide additional evidence for a higher metagalactic radiation field, $\Phi_0 \approx 10^4$ cm^{-2} s^{-1} and ionization rate $\Gamma_H \approx 8 \times 10^{-14}$ s^{-1}. These values, while still uncertain, are consistent with theoretical calculations (Haardt & Madau 2001; Shull et al. 1999) and inferences from the Lyα column-density distribution (Kollmeier et al. 2014; Egan et al. 2014).

Thus, the enhanced Si/C abundances are consistent with the PL, FG11, and HM05 radiation fields, but not with HM12. However, the constraints are not always in full agreement. Our choice of Δ_b is guided primarily by the need for sensible (finite and consistent) ionization correction factors for C and Si (Figures 5 and 6). Our inference of enhanced Si/C and softer radiation fields was also based on these consistency arguments. High radiation fields in the EUV and soft X-ray produce far too many high ions (C V, Si V, Si VI, Si VII) to be consistent with the expected metallicities. Because the high ionization states of Si are sensitive to hard-EUV and soft X-ray photons, the Si ionization correction curves in Figure 5 are too high for the HM12 radiation field, which has elevated fluxes between 3–300 Å. The bottom panel of Figure 5 shows that $\mathrm{CF_{Si}} > 10$ for $\Delta_b \leq 300$, inconsistent with the values of $\mathrm{CF_C}$ unless the Si/C abundance is enhanced above solar ratios. Figure 4 shows that the adjacent-ion ratios for C III/C IV and Si III/Si IV are somewhat inconsistent with the softer radiation backgrounds (FG11 and HM05), preferring the HM12 and PL distributions. Clearly, there is a need for additional work to infer the uncertain metagalactic background between 2–20 ryd, particularly between the He II edge (54.4 eV) and the soft X-ray band (0.3–3 keV) responsible for inner-shell ionization of many metal ions.

The total metal abundance, Ω_Z, can be estimated by dividing Ω_C, Ω_Si, and Ω_O by the individual mass fractions of these elements relative to all heavy elements. From the recent solar abundance calculations of Caffau et al. (2011), the relevant fractions are 18.2% (C), 4.34% (Si), and 44.0% (O). Using our corrections for ionization state and metal fractions of C and Si, we find mean mass densities of $\Omega_\mathrm{C} = 3.4 \times 10^{-7}$ and $\Omega_\mathrm{Si} = 2.1 \times 10^{-7}$. If we divide these parameters by the *solar* mass fractions of C (18.2%) and Si (4.34%), the photoionized Lyα-forest absorbers at low redshift traced by C III, C IV, Si III, and Si IV would correspond to total metal mass densities $\Omega_Z = 1.9 \times 10^{-6}$ from carbon or $\Omega_Z = 4.8 \times 10^{-6}$ from silicon. To make these two metallicity estimates consistent, we require Si/C to be enhanced by a factor of 3 relative to solar abundances. Such enhancements of alpha-process elements, [O/Fe] $\approx +0.5$, have also been seen in metal-poor halo stars (Åkerman et al. 2004) and in low-metallicity damped Lyα absorbers (Pettini et al. 2008). For example, in a survey of 20 metal-poor DLAs, Cooke et al. (2011) found a mean value [O/Fe] $= +0.39 \pm 0.12$.

We then re-calculate the metal fractions, enhancing the abundances by a factor of 3 for all alpha-process elements: even-Z nuclei from atomic number $Z = 8$ to 20 (O through Ca). The mass fractions become 7.95% (C), 5.70% (Si), and 58.0% (O), and the inferred metal abundances are $\Omega_Z = 4.3 \times 10^{-6}$ from carbon and $\Omega_Z = 3.7 \times 10^{-6}$ from silicon. With the Si/C enhancement, we infer a consistent value $\Omega_Z = (4.0 \pm 0.5) \times 10^{-6}$ in the photoionized gas, or a mass density $(5.4 \pm 0.7) \times 10^5$ $M_\odot$ Mpc^{-3}. We can perform a similar estimate of metal abundance from O VI, the single observed ion stage of oxygen. Numerous observations and models suggest that O VI can be formed from both photoionization and collisional ionization. As shown in Figure 7, the fraction of O VI from photoionization is expected to be small in the photoionized absorbers at $\Delta_b = 200 \pm 50$. In the hot gas, reflecting the fragility of its Li-like ionization state, the maximum O VI abundance fraction in collisional ionization equilibrium is $f_\mathrm{OVI} \approx 0.2$. Cosmological N-body hydrodynamic simulations (Smith et al. 2011; Shull et al. 2012) of the low-redshift IGM, accounting for both photoionization and collisional ionization, show that O VI exists in multiphase gas, with inhomogeneous distributions of metallicity ($Z/Z_\odot$) and ionization fraction f_OVI. In these calculations, the IGM-averaged product is $\langle (Z/Z_\odot) f_\mathrm{OVI} \rangle = 0.01$, a factor of 2 lower than the frequently assumed values of $Z/Z_\odot = 0.1$ and $f_\mathrm{OVI} = 0.2$. Here, we assume an ionization fraction $f_\mathrm{OVI} = \Omega_\mathrm{OVI}/\Omega_\mathrm{O} = 0.1$ and an oxygen-to-metals fraction $\Omega_\mathrm{O}/\Omega_Z = 0.58$, appropriate for all alpha-process elements enhanced by a factor of 3. The observed value in Table 2, $\Omega_\mathrm{OVI} = 38.6^{+4.8}_{-3.2}$ $(10^{-8} h_{70}^{-1})$ corresponds to $\Omega_\mathrm{O} = (3.9 \pm 0.5) \times 10^{-6}$ and total metal abundance $\Omega_Z = (6.7 \pm 0.8) \times 10^{-6}$. The metal density in the O VI-traced gas is $\rho_Z = (9.1 \pm 0.6) \times 10^5$ $M_\odot$ Mpc^{-3}.

For the total IGM metal density, we combine the values for photoionized gas (traced by the C and Si ions) with the hot gas (traced by O VI). The total metal density in both phases of the low-z IGM is $\rho_Z = (1.4 \pm 0.9) \times 10^6$ $M_\odot$ Mpc^{-3} or $\Omega_Z \approx 10^{-5}$. As we discuss in the next section, this corresponds to $\sim$10% of the expected heavy elements produced by cosmic star formation, integrated from $z \approx 8$ down to $z = 0$. The resulting metal density, $(1.5 \pm 0.8) \times 10^7$ $M_\odot$ Mpc^{-3}, is estimated from the integrated SFR density, $\rho_* = (6 \pm 2) \times 10^8$ $M_\odot$ Mpc^{-3}, assuming a mean metal yield $y_m = 0.025 \pm 0.010$.

3.4. *Metal Production History*

We now estimate the global metal-production, based on cosmological parameters and observations of the cosmic SFR history. Several groups have integrated the metal-production density. Pettini (1999) suggested that $\rho_Z \approx 4.5 \times 10^6$ $M_\odot$ Mpc^{-3} of metals were produced by $z = 2.5$, with a metal-production yield $y_m = 1/42$ from star formation between 11-13 Gyr. In a follow-up analysis, Pettini (2006) revised this to 3.4×10^6 $M_\odot$ Mpc^{-3} now assuming $y_m = 1/64$. Bouché et al. (2007) integrated the parameterized SFR history from Cole et al. (2001) with $y_m = 1/42$ to find 4×10^6 $M_\odot$ Mpc^{-3} down to $z = 2$ and 2.13×10^7 $M_\odot$ Mpc^{-3} down to $z = 0$.

In our current low-redshift IGM survey, we are interested in the star formation and metal production down to $z = 0$. We adopt somewhat larger error bars on ρ_* and ρ_Z that reflect systematic uncertainties in measuring the SFR history and computing the metal yield. These include a large (typically factor-of-five) dust correction to the SFR history applied between $1 < z < 4$ (Bouwens et al. 2011). Translating galaxy luminosity density into mass density also requires assumptions about the stel-

lar initial mass function (IMF), including its mass range, slope, and low-mass turnover. Similar assumptions affect the metal yield (Madau & Dickinson 2014) which can range from $y_m = 0.016 - 0.032$ for a Salpeter or Chabrier IMF counting the metals produced by massive stars between $10 - 40\ M_\odot$. Metal contributions from higher mass stars are cut off by core collapse into black holes. The range increases to $y_m = 0.023 - 0.048$ if the black hole cutoff is raised to 60 $M_\odot$. Studies of the dependence of metal production on cutoff (Brown & Woosley 2013) suggest a range $25\ M_\odot < M_{\rm BH} < 60\ M_\odot$. Some of the uncertainty in metal production is offset with the conversion from UV light to mass, since the same massive stars produce both UV photons and metals (Madau & Shull 1996).

Adding appropriate uncertainties in the SFR measurements and dust corrections, we adopt an integrated stellar mass density $\rho_* \approx (6 \pm 2) \times 10^8\ M_\odot\ {\rm Mpc}^{-3}$. In their review, Madau & Dickinson (2014) quote $\rho_* = 5.8 \times 10^8\ M_\odot\ {\rm Mpc}^{-3}$ from their model SFR history, in good agreement with the value $(6.0 \pm 1.0) \times 10^8\ M_\odot\ {\rm Mpc}^{-3}$ found by Gallazzi et al. (2008). As a final check, we integrated the SFR history (Bouwens et al. 2011) from $z = 8$ to the present. Over the past 10 Gyr, the SFR density, expressed in units $M_\odot\ {\rm yr}^{-1}\ {\rm Mpc}^{-3}$, falls dramatically, from $\dot\rho_* \approx 0.1$ at $t = 10$ Gyr ($z = 1.76$) to $\dot\rho_* \approx 0.01$ ($z \approx 0$). The SFR density is well-fitted in look-back time (t) over the range $0 < t < 10$ Gyr by $\log \dot\rho_* = -2.0 + (t/10\ {\rm Gyr})$, equivalent to the exponential form:

$$\dot\rho_* = (0.01\ M_\odot\ {\rm yr}^{-1}\ {\rm Mpc}^{-3})\ \exp\left[2.3026\,(t/10\ {\rm Gyr})\right]. \quad (11)$$

Integrated back to 10 Gyr ($0 < z < 1.76$), this gives a total density of star formation, $\rho_* = (0.01)(10^{10}\ {\rm yr})(9/2.3026) = 3.9 \times 10^8\ M_\odot\ {\rm Mpc}^{-3}$. From $t = 10 - 11$ Gyr ($1.76 < z < 2.4$) the SFR density is near its peak value ($0.1\ M_\odot\ {\rm yr}^{-1}\ {\rm Mpc}^{-3}$) and contributes $\sim 1 \times 10^8\ M_\odot\ {\rm Mpc}^{-3}$. The declining star formation from $z = 2.4$ to $z \approx 8$ (Bouwens et al. 2011) adds a similar metal density, for an integrated total of $6 \times 10^8\ M_\odot\ {\rm Mpc}^{-3}$.

Taking into account uncertainties in IMF and metal production, we adopt a metal yield $y_m = 0.025 \pm 0.010$ and predict an integrated metal density $\rho_Z = (1.5 \pm 0.8) \times 10^7 M_\odot\ {\rm Mpc}^{-3}$. This corresponds to a fractional metal density $\Omega_Z = (1.1 \pm 0.7) \times 10^{-4}$ with combined uncertainties in integrated SFR and metal yield. Some of these metals stay locked into stellar remnants, others remain within the galactic interstellar medium, and some are blown into the CGM and IGM. Estimates of the metal fractions in these components range from 60-70% (Bouché et al. 2007; Peeples et al. 2014). For the CGM and IGM surveys, the primary issues are: (1) How many metals were expelled by galactic winds? (2) In what thermal phase and ionization state do they reside? (3) How many metals are undetected owing to their existence in higher ionization states?

A considerable mass of metals resides in the halos of galaxies, in the CGM, and probably gas expelled to the IGM. We estimate the galactic-halo contribution from the luminosity function of the Millennium Survey (Driver et al. 2005) with their Schechter-function parameters ($\phi^* = 0.0177 h^3\ {\rm Mpc}^{-3}$, $\alpha = -1.13$). We compute a galaxy space density $3.8 \times 10^{-3}\, h_{70}^3\ {\rm Mpc}^{-3}$, converting from h to h_{70} and integrating between $0.5 - 1.5 L^*$ (effective bandwidth of $0.63 L^*$). We multiply by an estimated fraction, $f_{\rm SF} \approx 0.3$, of active star-forming galaxies and the mean mass of metals per halo, $2.65 \times 10^7\ M_\odot$, found in O VI absorbers from the COS-Halos study (Tumlinson et al. 2011, 2013) and scaled to total metals using the likely range of oxygen mass fractions ($50 \pm 10\%$). We obtain a metal density $\rho_Z \approx 3 \times 10^4\ M_\odot\ {\rm Mpc}^{-3}$ corresponding to $\Omega_Z \approx 2 \times 10^{-7}$. This is only a small fraction of the cosmic metal production, but there are large uncertainties in these estimates. The star-forming fraction $f_{\rm SF}$ depends on which stellar mass M^* one chooses (Ilbert et al. 2013; Baldry et al. 2012), while the integrated SFR, with its dust correction, is probably uncertain by a factor of 2 (Karim et al. 2011; Madau & Dickinson 2014).

Our best estimate is that the low-z IGM contains $10 \pm 5\%$ of the cosmic metals, which agrees with estimates for the metal abundance in various thermal phases of the IGM. For example, we can combine the mean IGM metallicity, $Z_{\rm IGM}$ to the solar metallicity, $Z_\odot \approx 0.0153$ by mass (Caffau et al. 2011) with the cosmological baryon density, $\Omega_b \approx 0.0461$, measured by microwave background experiments (Hinshaw et al. 2013). Our recent baryon census (Shull et al. 2012) found that the low-z Lyα forest contains $28 \pm 11\%$ of the baryons, with the shock-heated WHIM traced by O VI and broad Lyα absorbers containing $25 \pm 8\%$. The expected metal densities in the Lyα forest and O VI-traced WHIM would then be

$$\Omega_Z^{\rm (Lya)} \approx 0.28\,\Omega_b\,Z_{\rm IGM} \approx (2.0 \times 10^{-6}) \left(\frac{Z_{\rm IGM}}{0.01 Z_\odot}\right)$$
$$\Omega_Z^{\rm (WHIM)} \approx 0.25\,\Omega_b\,Z_{\rm IGM} \approx (1.8 \times 10^{-6}) \left(\frac{Z_{\rm IGM}}{0.01 Z_\odot}\right) \quad (12)$$

In our survey, the observed ion states (C III, C IV Si III, Si IV) with ionization corrections suggested that 4% of the cosmic metals reside in the photoionized IGM, with an additional 6% in hotter gas traced by O VI. The inferred metal densities were $(5.4 \pm 0.7) \times 10^5\ M_\odot\,{\rm Mpc}^{-3}$ or $\Omega_Z = (4 \pm 0.5) \times 10^{-6}$ for the Lyα absorbers and $(9.1 \pm 0.6) \times 10^5\ M_\odot\,{\rm Mpc}^{-3}$ or $\Omega_Z = (6.7 \pm 0.5) \times 10^{-6}$ for the O VI-traced WHIM. These densities correspond to mean metallicities of 2% solar (Lyα forest) and 4% solar (WHIM), both with substantial uncertainty from the ionization corrections. One expects large variations in the IGM metallicity owing to incomplete metal transport and mixing.

Finally, it is appropriate to ask whether the ions in this survey can be described, in either photoionization or collisional ionization equilibrium, with the alpha-enhanced abundance pattern as discussed above. Most observations and cosmological simulations suggest that the low-z IGM absorbers are multi-phase gas, with contributions from photoionization at $T \approx 10^4$ K (for H I, C III, C IV, Si III, Si IV) and hotter, shock-heated gas at

$T \approx 10^{5.5\pm0.5}$ K containing much of the O VI. The oxygen ionization correction is less certain than those of C and Si; some of the O VI may be photoionized and double-counted in the Lyα forest traced by C and Si ions. Below, we compare ratios of the *observed* ion states for the elements (O/C), (O/Si), (C/Si), (N/C), and (N/O) to their values assuming relative solar abundances:

$$\begin{aligned}
(\mathrm{O/C}) &= \Omega_{\mathrm{OVI}}/(\Omega_{\mathrm{CIII}} + \Omega_{\mathrm{CIV}}) \approx 2.24^{+0.80}_{-0.40} \\
(\mathrm{O/Si}) &= \Omega_{\mathrm{OVI}}/(\Omega_{\mathrm{SiIII}} + \Omega_{\mathrm{SiIV}}) \approx 11.0^{+3.5}_{-1.9} \\
(\mathrm{C/Si}) &= (\Omega_{\mathrm{CIII}} + \Omega_{\mathrm{CIV}})/(\Omega_{\mathrm{SiIII}} + \Omega_{\mathrm{SiIV}}) \approx 4.9^{+2.2}_{-1.1} \\
(\mathrm{N/C}) &= \Omega_{\mathrm{NV}}/(\Omega_{\mathrm{CIII}} + \Omega_{\mathrm{CIV}}) \approx 0.11^{+0.05}_{-0.03} \\
(\mathrm{N/O}) &= \Omega_{\mathrm{NV}}/\Omega_{\mathrm{OVI}} \approx 0.049^{+0.017}_{-0.011} \qquad (13)
\end{aligned}$$

For reference, the solar mass-abundance ratios can be derived from the abundances by number (Caffau et al. 2011): $\rho_{\mathrm{O}}/\rho_{\mathrm{C}} = (16/12)(n_{\mathrm{O}}/n_{\mathrm{C}}) = 2.43$, $\rho_{\mathrm{O}}/\rho_{\mathrm{Si}} = (16/28)(n_{\mathrm{O}}/n_{\mathrm{Si}}) = 8.65$, $\rho_{\mathrm{C}}/\rho_{\mathrm{Si}} = (12/28)(n_{\mathrm{C}}/n_{\mathrm{Si}}) = 4.18$, $\rho_{\mathrm{N}}/\rho_{\mathrm{C}} = (14/12)(n_{\mathrm{N}}/n_{\mathrm{C}}) = 0.25$, and $\rho_{\mathrm{N}}/\rho_{\mathrm{O}} = (14/16)(n_{\mathrm{N}}/n_{\mathrm{O}}) = 0.12$. From photoionization modeling of the C and Si ions[4] we only obtain a consistent metallicity if Si/C is enhanced by a factor of 3 over solar values. The (O/C) and (C/Si) ratios are comparable to the solar abundances (Asplund et al. 2009; Caffau et al. 2011), while the (O/Si) ratio is somewhat larger. As often is the case, N is underabundant relative to both C and O, although with just a single measured ion state (N V and O VI) these ratios are not necessarily accurate indicators of total abundances. However, the observed mass-density ratio, $\Omega_{\mathrm{NV}}/\Omega_{\mathrm{OVI}} \approx 0.049$ may indicate that (N/O) $\approx$ 40% of the solar ratio. From an analysis (Pettini & Cooke 2012) of the nitrogen metallicity dependence on primary and secondary nucleosynthesis, this ratio suggests that the sources of this gas likely had metallicity well above the metal-poor floor at $\log(\mathrm{N/O}) = -2.3$.

4. CONCLUSIONS AND DISCUSSION

A fundamental uncertainty in any "missing metals" survey is set by estimates of the total metal production rates from the integrated SFR history and metal yields. Our UV survey finds that the low-z IGM contains 10$\pm$5% of the metal density $\rho_Z = (1.5 \pm 0.8) \times 10^7\ M_\odot\ \mathrm{Mpc}^{-3}$ integrated to $z = 0$. The bulk of the metals are likely contained in stars and ISM within galaxies (Bouchè et al. 2007) and in hot gas in galactic halos and the CGM (Peeples et al. 2014). The efficiency of metal transport is still uncertain, as recently injected metals may not extend from their galactic sources, given the outflow speeds and finite lifetimes of the flows (Oppenheimer & Davé 2008). Thus, it is no surprise that only 10% of the metals have made it into the IGM, with many more located in galaxy halos and the CGM (Tumlinson et al. 2013; Stocke et al. 2013).

Our *HST*/COS survey of QSO metal-line absorbers provides the largest current sample of metallicity in the low-redshift IGM. Of particular importance are abundances of adjacent ion stages, whose ratios C III/C IV and Si III/Si IV improve the ionization corrections. Because the production of high ions of C and Si have different dependences on EUV and X-ray photons, their individual ionization corrections constrain the ionizing background and baryon overdensity. We correct the measured ion densities of the adjacent ion states, $(\Omega_{\mathrm{CIII}} + \Omega_{\mathrm{CIV}})$ and $(\Omega_{\mathrm{SiIII}} + \Omega_{\mathrm{SiIV}})$, by factors $\Omega_{\mathrm{C}}/[\Omega_{\mathrm{CIII}} + \Omega_{\mathrm{CIV}}] = 2.0^{+1.0}_{-0.5}$ and $\Omega_{\mathrm{Si}}/[\Omega_{\mathrm{SiIII}} + \Omega_{\mathrm{SiIV}}] = 6^{+4}_{-3}$ to derive elemental mass densities $\Omega_{\mathrm{C}} = 3.4 \times 10^{-7}$ and $\Omega_{\mathrm{Si}} = 2.1 \times 10^{-7}$. Consistency of the C and Si metallicities requires that Si/C be enhanced by a factor 3 over solar abundances. Presumably, other alpha-process elements (even-Z nuclei from O through Ca) are also enhanced. The inferred Si/C enhancement in the low-z IGM suggests that these metals were injected at the peak of star formation ($z \approx 1-3$) by young stellar populations whose massive stars provided alpha-process nucleosynthesis.

The total metal abundance in the low-z, photoionized Lyα forest absorbers is $\Omega_Z = (4.0 \pm 0.5) \times 10^{-6}$, consistent with the individual values $\Omega_Z = 4.3 \times 10^{-6}$ inferred from carbon and $\Omega_Z = 3.7 \times 10^{-6}$ from silicon. A similar exercise for O VI gives $\Omega_{\mathrm{O}} = 3.9 \times 10^{-6}$ and $\Omega_Z = 6.7 \times 10^{-6}$. Because O VI likely traces a different thermal phase than the photoionized C and Si ions, these two densities are additive, yielding a total IGM metal density of $\Omega_Z \approx 10^{-5}$. This density is $\sim$10% of the metals produced by cosmic star formation. Additional metals reside in the halos and CGM of galaxies as probed in absorption lines of O VI (Tumlinson et al. 2013), C IV (Borthakur et al. 2013), and Ca II (Zhu & Ménard 2013). Quantitative estimates of the total metal content in these reservoirs will require UV and X-ray absorption-line measurements that cover the range of ionization states in this multiphase gas (Stocke et al. 2013; Werk et al. 2014) located 50-300 kpc from galaxies, both within and beyond their virial radii (Shull 2014).

[4] Because the ionization corrections for C and Si respond in different ways to EUV and X-ray photoionization (see Appendix B), the Si/C abundance ratio inferred from just the two observed ion states, C III and C IV compared to Si III and Si IV, is not an accurate measure of the total abundances.

The primary conclusions of our low-redshift IGM metal survey are as follows:

1. For six metal ions in the IGM surveyed by HST/COS spectra (Danforth et al. 2014) at $\langle z \rangle \approx 0.14$, we find cosmic mass densities $\Omega_{\rm ion} \equiv \rho_{\rm ion}/\rho_{\rm cr}$ (in units $10^{-8}\,h_{70}^{-1}$) of $\Omega_{\rm CIV} = 10.1^{+5.6}_{-2.4}$, $\Omega_{\rm CIII} = 7.1^{+1.9}_{-1.2}$, $\Omega_{\rm OVI} = 38.6^{+4.8}_{-3.2}$, $\Omega_{\rm SiIV} = 2.1^{+1.0}_{-0.5}$, $\Omega_{\rm SiIII} = 1.4^{+0.3}_{-0.2}$, and $\Omega_{\rm NV} = 1.9^{+0.6}_{-0.4}$ integrated over column density ranges specified in Table 2.

2. Our survey includes key intermediate ion stages (C III and Si III) as well as C IV and Si IV. The mean mass-abundance ratios of the survey, C III/C IV $\approx 0.70^{+0.43}_{-0.20}$ and Si III/Si IV $\approx 0.67^{+0.35}_{-0.19}$, are consistent with a metagalactic ionizing background with photoionization parameter $\log U = -1.5 \pm 0.4$. A suite of photoionization models yields correction factors for higher ion stages and requires that Si/C be enhanced by a factor of 3 above solar abundances.

3. Applying photoionization corrections to (C III + C IV) and (Si III + Si IV), we estimate a metal density of $\Omega_Z \approx (4.0 \pm 0.5) \times 10^{-6}$ or 4% of the predicted metal production. For hot IGM traced by O VI, we find $\Omega_Z \approx (6.7 \pm 0.8) \times 10^{-6}$ or 6% of the metal production. Combining the two reservoirs, we estimate that the low-z IGM contains $10 \pm 5\%$ of the total metal production, $(1.5 \pm 0.8) \times 10^7\ M_\odot$ Mpc^{-3}, predicted from integrated star formation, $(6 \pm 2) \times 10^8\ M_\odot$ Mpc^{-3} with yields $y_m \approx 0.025 \pm 0.010$.

4. For several ionization backgrounds (at $z \approx 0$), our photoionization models of the metal absorbers are consistent with a soft ionizing background above the He II edge with ionizing intensity $I_0 = (3 \pm 1) \times 10^{-23}$ erg cm^{-2} s^{-1} Hz^{-1} sr^{-1} at the hydrogen Lyman limit. These backgrounds correspond to one-sided ionizing flux $\Phi_0 \approx 10^4$ cm^{-2} s^{-1} and hydrogen ionization rate $\Gamma_{\rm H} \approx (8 \pm 2) \times 10^{-14}$ s^{-1}. These values need additional observational constraints, but they are consistent with previous theoretical calculations (Haardt & Madau 2001; Shull et al. 1999) and inferences from the Lyα column-density distribution (Kollmeier et al. 2014; Egan et al. 2014).

5. The photoionization parameter $\log U = -1.5 \pm 0.4$ with baryon overdensities $\Delta_b \approx 200 \pm 50$ and Si/C = 3 times solar abundances. This overdensity corresponds to $n_H \approx 10^{-4.25 \pm 0.10}$ cm^{-3} at $\langle z \rangle = 0.14$, a hydrogen gas density typical of that in extended galactic halo gas.

6. Given the uncertainties in integrated SFR and metal production and the demonstrated existence of reservoirs of metals (galactic stars, galaxy halos, CGM, and hotter gas), there is probably no compelling reason to require a missing metals problem. Further UV and X-ray measurements of these galactic and CGM reservoirs and their ionization conditions will be needed to quantify this metal census.

Looking toward future improvements in these metal surveys, we note the uncertainties in the metal-ion column density distributions at the high end: $\log N > 15.0$ (C IV and O VI), $\log N > 13.5$ (Si III), $\log N > 14.0$ (Si IV), and $\log N > 14.5$ (C III). From power-law fits to these CDDFs, we see that better characterization would be most useful for Si IV, N V, and Si III. The Si abundances are less secure than those of C, owing to a smaller number of Si IV absorbers and consistent with the scatter in low-z measurements of $\Omega_{\rm SiIV}$ (Danforth & Shull 2008; Cooksey et al. 2011; Tilton et al. 2012; Danforth et al. 2014). The total redshift pathlengths in the medium-resolution COS bands (G130M and G160M) from 1135-1796 Å vary considerably by ion: $\Delta z \approx 20$ (H I), 18 (Si III), 13 (Si IV), 17 (N V), 13 (O VI), 10 (C III), and 8 (C IV). The lines of C IV and Si IV redshift out of the G160M band at $z > 0.16$ and $z > 0.29$ respectively. Longer wavelength *HST* surveys would require considerably more observing time with less efficient gratings. Additional ionization states would also help to characterize the ionization modeling. In the UV, surveys of the lower ions (C II and Si II) would complement our measurements of intermediate ion states (C III, C IV, Si III, Si IV). To better constrain the uncertain high-energy background radiation and inner-shell ionization, it would be helpful to observe the expected higher ion states in X-ray absorbers (C V, C VI, O VII, O VIII, Si V, Si VI, Si VII).

We thank George Becker, Alec Boksenberg, Bob Carswell, Mark Giroux, Max Pettini, and Joop Schaye for helpful discussions and comments on metal-line measurements in the IGM and ionizing backgrounds. This research was supported by the STScI COS grant (NNX08-AC14G) at the University of Colorado Boulder. JMS thanks the Institute of Astronomy at Cambridge University for their stimulating scientific environment and support through the Sackler Visitor Program.

APPENDIX

APPENDIX A: ANALYTIC ESTIMATES OF $\Omega_{\rm ION}$

Equation (1) gives an expression for the mass density of an ion, involving an integral over the column density distribution function (CDDF), denoted by $f(N,z) \equiv (\partial^2\mathcal{N}/\partial N\,\partial z)$. In our IGM survey (Danforth et al. 2014), we fitted the cumulative distribution of column densities (N) to a power law,

$$\frac{d\mathcal{N}(>N)}{dz} = C_0 \left(\frac{N}{N_0}\right)^{-(\beta-1)} \quad , \tag{A1}$$

where C_0 is the normalization at fiducial column density $N_0 = 10^{14}$ cm^{-2}. For several ions (O VI and C IV) we fitted piecewise continuous power laws, for strong and weak absorbers. We obtain the CCDF by differentiating the cumulative distribution with respect to N,

$$f(N,z) = \frac{C_0(\beta-1)}{N_0}\left(\frac{N}{N_0}\right)^{-\beta} \quad . \tag{A2}$$

With $x = N/N_0$ and $N_0 = 10^{14}$ cm^{-2}, the fractional ion density becomes

$$\begin{aligned}\Omega_{\rm ion} &= (1.365\times10^{23}\ h_{70}^{-1}\,{\rm cm}^2)\left(\frac{m_{\rm ion}}{\rm amu}\right)\int_{\rm N_{min}}^{\rm N_{max}} \frac{C_0(\beta-1)}{N_0}\left(\frac{N}{N_0}\right)^{-\beta} N\,dN \\ &= (1.365\times10^{-9}\ h_{70}^{-1})\,C_0(\beta-1)\left(\frac{m_{\rm ion}}{\rm amu}\right)\int_{\rm x_{min}}^{\rm x_{max}} x^{-(\beta-1)}\,dx \ , \end{aligned} \tag{A3}$$

an expression that can be evaluated for each of the segments of the CCDF fits. From this integral, we see that distributions with $\beta < 2$ are dominated by high-N absorbers (near $N_{\rm max}$) while expressions with $\beta > 2$ are dominated by low-N absorbers (near $N_{\rm min}$).

$$\Omega_{\rm ion} = (1.365\times10^{-9}\ h_{70}^{-1})\,C_0\left(\frac{\beta-1}{\beta-2}\right)\left(\frac{m_{\rm ion}}{\rm amu}\right)\left[x_{\rm min}^{-(\beta-2)} - x_{\rm max}^{-(\beta-2)}\right] \quad ({\rm for}\ \beta>2) \tag{A4}$$

$$\Omega_{\rm ion} = (1.365\times10^{-9}\ h_{70}^{-1})\,C_0\left(\frac{\beta-1}{2-\beta}\right)\left(\frac{m_{\rm ion}}{\rm amu}\right)\left[x_{\rm max}^{(2-\beta)} - x_{\rm min}^{(2-\beta)}\right] \quad ({\rm for}\ \beta<2) \tag{A5}$$

$$\Omega_{\rm ion} = (1.365\times10^{-9}\ h_{70}^{-1})\,C_0\left(\frac{m_{\rm ion}}{\rm amu}\right)\ln\left(\frac{x_{\rm max}}{x_{\rm min}}\right) \quad ({\rm for}\ \beta=2) \tag{A6}$$

Table 3 gives the fitting parameters (C_0, β) for the metal six ions in our survey and the resulting values of $\Omega_{\rm ion}$, which can be compared with the discrete numerical integrals over logarithmic bins, $\Delta\log N = 0.2$, given in Table 2.

APPENDIX B: PHOTOIONIZATION RATES AND IONIZING FLUXES

In this Appendix we discuss analytic approximation to the equilibrium ionization ratios of high ions of C and Si. In the approximation that each ionization stage of an element is coupled only to those immediately above and below, the ionization fractions, f_i, can be derived by solving pairwise along the "rungs of the ladder". Consider two adjacent ion stages, Si IV and Si V, in photoionization equilibrium with abundance ratio $n_{\rm SiV}/n_{\rm SiIV} \approx (\Gamma_{\rm SiIV}/n_e\alpha_{\rm SiIV})$. Here, $\Gamma_{\rm SiIV}$ (s^{-1}) is the photoionization rate of Si IV and $\alpha_{\rm SiIV}$ (cm^3 s^{-1}) is the recombination rate coefficient from Si V to Si IV. For an isotropic radiation field with specific intensity of power-law form, $I_\nu = I_i(\nu/\nu_T)^{-\alpha}$, at energies $h\nu \geq h\nu_T$ above the ionization threshold ($E_T = h\nu_T$) of Si IV, and for photoionization cross sections fitted to power-law form, $\sigma_\nu = \sigma_T(\nu/\nu_T)^{-\beta}$, one can derive the photoionization rate,

$$\Gamma_{\rm SiIV} = 4\pi \int_{\nu_0}^{\infty} \frac{I_\nu \sigma_\nu}{h\nu}\, d\nu = \frac{4\pi I_i \sigma_i}{h(\alpha+\beta)} = (1.90\times10^{-14}\ {\rm s}^{-1}) \left[\frac{I_{-23}\,\xi_{\rm SiIV}}{(\alpha+\beta)}\right] \left(\frac{\sigma_T}{\rm Mb}\right)\ . \tag{B1}$$

The photoionization cross section is scaled to a threshold value of 1 Mb (10^{-18} cm^2), where a fit to the Si IV tabulation by Verner et al. (1996) gives $\sigma_T = 0.314$ Mb and $\beta \approx 1.15$ between E_T and $1.4E_T$. The intensity at the Si IV threshold ($E_T = 45.14$ eV) is written $I_i = J_0\,\xi_{\rm SiIV}$, reduced by a factor $\xi_{\rm SiIV}$ from its value $I_0 = (10^{-23}$ erg cm^{-2} s^{-1} Hz^{-1} sr^{-1})J_{-23} at the hydrogen Lyman limit ($h\nu_0 = 13.60$ eV). For a power-law radiation field, $\xi_{\rm SiIV} = (\nu_{\rm SiIV}/\nu_0)^{-\alpha} \approx 0.186$ for $\alpha = 1.4$, and $\Gamma_{\rm SiIV} = (4.35\times10^{-16}\ {\rm s}^{-1})I_{-23}(\xi_{\rm SiIV}/0.186)$. The recombination rate coefficient at temperature $T = (10^4\ {\rm K})T_4$ is approximated (Shull & Van Steenberg 1982) as $\alpha_{\rm SiIV} \approx (5.5\times10^{-12}$ cm^3 s^{-1})$T_4^{-0.821}$. The electron density in the IGM absorber $n_e = 1.167\bar{n}_H\Delta_b = (2.22\times10^{-7}\ {\rm cm}^{-3})\Delta_b$, for overdensity $\Delta_b = 100\Delta_{100}$ and fully ionized helium with abundance $y = n_{\rm He}/n_{\rm H} = 0.0833$. Thus, for $(\alpha+\beta) = 2.55$, we have

$$\frac{n_{\rm SiV}}{n_{\rm SiIV}} = \frac{\Gamma_{\rm SiIV}}{n_e\alpha_{\rm SiIV}} \approx (3.6) I_{-23}\,\Delta_{100}^{-1}\,T_4^{0.821}\,(\xi_{\rm SiIV}/0.186)\ . \tag{B2}$$

One can perform the same exercise for the Si V and Si VI pair, where a fit to Si V photoionization cross sections (Verner et al. 1996) gives $\sigma_T = 2.61$ Mb at threshold, $E_T = 166.77$ eV, rising to 3.2-3.4 Mb between 170-200 eV, and then declining from 200-300 eV with $\sigma_\nu \propto \nu^{-2.1}$. The recombination rate coefficient $\alpha_{\rm SiV} = (1.2\times10^{-11}$ cm^3 s^{-1})$T_4^{-0.735}$ and the Si V flux-reduction factor is $\xi_{\rm SiV} = (166.77/13.60)^{-1.4} \approx 0.030$. We estimate that $\Gamma_{\rm SiV} \approx (5.6\times10^{-16}\ {\rm s}^{-1})(\xi_{\rm SiV}/0.030)$ and

$$\frac{n_{\rm SiVI}}{n_{\rm SiV}} = \frac{\Gamma_{\rm SiV}}{n_e\alpha_{\rm SiV}} \approx (2.1) I_{-23}\,\Delta_{100}^{-1}\,T_4^{0.735}\,(\xi_{\rm SiV}/0.030)\ . \tag{B3}$$

Evidently, Si V and Si VI are likely to have significant ionization fractions for $\Delta_b \leq 100$, if the ionizing radiation field falls off as a power law, $(\nu/\nu_0)^{-\alpha}$ at $h\nu \gg 1$ ryd above the Si IV and Si V edges. Inner-shell ionization by X-rays above the K-edges, 1910 eV, 1930 eV, and 1950 eV for Si III, Si IV, and Si V, respectively, followed by Auger electron emission (Weisheit 1974; Donahue & Shull 1991) will enhance the Si V and Si VI abundances. Following K-shell ionization, Si III will jump to Si VI or Si VII with 2 or 3 Auger electrons released depending on whether the inner-shell (1s) vacancy is filled by a *2s* or *2p* electron. The difference arises because of valence (3s) electrons, which can be released when a *2p* electron drops into a *2s* vacancy. Similarly, a K-shell ionization of Si IV will release either 1 or 2 Auger electrons, producing Si VI or Si VII.

Carbon, with fewer electrons, offers a somewhat different response to K-shell ionization, with threshold energies at 296 eV, 317 eV, and 347 eV for C II, C III, and C IV, respectively. With three electrons, C IV (*1s^2 2s*) will release no Auger electrons to fill the K-shell vacancy, but C III (*1s^2 2s^2*) will release a single *2s* electron through the Auger process. Thus, inner-shell ionization of C III and C IV will both produce C V. For C IV valence-shell (*2s*) photoionization, $\sigma_T = 0.656$ Mb at $E_T = 64.49$ eV, and $\beta \approx 1.7$ between E_T and $1.4E_T$ from the tabulated cross sections (Verner et al. 1996). The radiative recombination rate coefficient $\alpha_{\rm CIV} \approx (7.5\times10^{-12}$ cm^3 s^{-1})$T_4^{-0.817}$. Thus, for a $\nu^{-1.4}$ ($\alpha = 1.4$) radiation field, a flux-reduction factor $\xi_{\rm CIV} = (64.49/13.60)^{-1.4} \approx 0.113$, and $(\alpha+\beta) = 3.5$, the photoionization rate $\Gamma_{\rm CIV} \approx (4.54\times10^{-16}\ {\rm s}^{-1})I_{-23}\ (\xi_{\rm CIV}/0.113)$ and we have

$$\frac{n_{\rm CV}}{n_{\rm CIV}} = \frac{\Gamma_{\rm CV}}{n_e\alpha_{\rm CIV}} \approx (2.7) I_{-23}\,\Delta_{100}^{-1}\,T_4^{0.817}\,(\xi_{\rm CIV}/0.113)\ . \tag{B4}$$

REFERENCES

Adams, J. J., Uson, J. M., Hill, G. J., & MacQueen, P. J. 2011, ApJ, 728, 107
Akerman, C.J., Carigi, L., Nissen, P. E., Pettini, M., & Asplund, M. 2005, A&A, 414, 931
Aguirre, A., Schaye, J., Kim, T.-S., et al. 2004, ApJ, 602, 38
Asplund, M., Grevesse, N., Sauval, A. J., & Scott, P. 2009, ARA&A, 47, 481
Aver, E.., Olive, K. A., & Skillman, E. D. 2013, JCAP, 11, 17
Baldry, I. K., Driver, S. P., Loveday, J., et al. 2012, MNRAS, 421, 621
Becker, G. D., Rauch, M., & Sargent, W. L. W. 2009, ApJ, 698, 1010
Boksenberg, A., Rauch, M., & Sargent, W. L. W. 2003, arXiv:astro-ph/0307557
Boksenberg, A., & Sargent, W. L. W. 2014, ApJS, in press
Borthakur, S., Heckman, T., Strickland, D., Wild, V., & Schiminovich, D. 2013, ApJ, 768, 18
Bouché, N., Lehnert, M. D., Aguirre, A., Peroux, C., & Bergeron, J. 2007, MNRAS, 378, 525
Bouwens, R. J., Illingworth, G, P., Oesch, P. A., et al. 2011, ApJ, 737, 90
Brown, J. M., & Woosley, S. E. 2013, ApJ, 769, 99
Caffau, E., Ludwig, H.-G., Steffen, M., Freytag, B., & Bonifacio, P. 2011, Solar Physics, 268, 255
Churazov, E., Sunyaev, R., Revnivtsev, M., et al. 2007, A&A, 467, 529
Cole, S., Norberg, P., Baugh, C. M., et al. 2001, MNRAS, 326, 255
Cooke, R., Pettini, M., Steidel, C. C., Rudie, G. C., & Nissen, P. E. 2011, MNRAS, 417, 1534
Cooksey, K. L., Thom, C., Prochaska, J. X., & Chen, H.-W. 2010, ApJ, 708, 868
Cooksey, K. L., Prochaska, J. X., Thom, C., & Chen, H.-W. 2011, ApJ, 729, 87
Cooksey, K. L., Kao, M., Simcoe, R., O'Meara, J. M., & Prochaska, J. X. 2013, ApJ, 763, 37
Danforth, C. W., & Shull, J. M. 2005, ApJ, 624, 555
Danforth, C. W., & Shull, J. M. 2008, ApJ, 679, 194
Danforth, C. W., Tilton, E. M., Shull, J. M., et al. 2014, ApJ, submitted (arXiv:1402.2655)
Davé, R., Hernquist, L., Katz, N., & Weinberg, D. H. 1999, ApJ, 511, 521
D'Odorico, V., Calura, F., Cristiani, S., & Viel, M. 2010, MNRAS, 401, 2715
D'Odorico, V., Cupani, G., Cristiani, S., et al. 2013, MNRAS, 435, 1198
Donahue, M., & Shull, J. M. 1991, ApJ, 383, 511
Donahue, M., Aldering, G., & Stocke, J. T. 1995, ApJ, 450, L45
Dove, J. B., & Shull, J. M. 1994, ApJ, 423, 196
Driver, S. P., Liske, J., Cross, N. J. G., De Propris, R., & Allen, P. D. 2005, MNRAS, 360, 81
Egan, H. , Smith, B. D., O'Shea, B. W., & Shull, J. M. 2014, ApJ, 791, 64
Faucher-Giguère, C-A., Lidz, A., Zaldarriaga, M., & Hernquist, L. 2009, ApJ, 703, 1416
Ferland, G. J., Porter, R. L., van Hoof, P. A. M., et al. 2013, Revista Mexicana A&A, 49, 1
Ferrara, A., Scannapieco, E., & Bergeron, J. 2005, ApJ, 634, L37
Gallazzi, A., Brinchmann, J., Charlot, S., & White, S. D. M. 2008, MNRAS, 383, 1439
Green, J. C., Froning, C., Osterman, S., et al. 2012, ApJ, 744, 60
Haardt, F., & Madau, P. 1996, ApJ, 461, 20
Haardt, F., & Madau, P. 2001, arXiv:astro-ph/0106018
Haardt, F., & Madau, P. 2012, ApJ, 746, 125
Hasinger, G. 1994, in Frontiers of Space and Ground-Based Astronomy: The Astrophysics of the 21st Century, ed. W. Wamsteker, M. Longair, & Y. Kondo (Astrophysics and Space Science Library, Vol. 187; Dordrecht: Kluwer), 381
Hinshaw, G., Larson, D., Komatsu, E., et al. 2013, ApJS, 208, 19
Ilbert, O., McCracken, H. J., Le Fèvre, O., et al. 2013, A&A, 556, A55
Karim, O., Schinnerer, E., Martinez-Sansigre, A., et al. 2011, ApJ, 730, 61
Kollmeier, J. A., Weinberg, D. H., Oppenheimer, B. D., et al. 2014, ApJ, 789, L32
Madau, P., & Shull, J. M. 1996, ApJ, 457, 551
Madau, P., & Dickinson, M. 2014, ARA&A, 52, in press (arXiv:1403.0007)
Morton, D. C. 2003, ApJS, 149, 205
Oppenheimer, B. D., & Davè, R. 2008, MNRAS, 387, 577
Peeples, M. S., Werk, J. K., Tumlinson, J., et al. 2014, ApJ, 786, 54
Penton, S., Stocke, J. T., & Shull, J. M. 2000, ApJ, 544, 150
Penton, S., Stocke, J. T., & Shull, J. M. 2004, ApJS, 152, 29
Pettini, M. 1999, in Proc. ESO Workshop, Chemical Evolution from Zero to High Redshift, ed. J. R. Walsh & M. R. Rosa, (Berlin: Springer), 233
Pettini, M. 2006, in The Fabulous Destiny of Galaxies: Bridging Past and Present, ed., V. LeBrun, A. Mazure, S. Arnouts, D. Burgarella (Paris: Frontier Group), 319
Pettini, M., & Cooke, R. 2012, in XII International Symposium on Nuclei in the Cosmos, Cairns, Australia, published on-line (arXiv:1209.4783)
Pettini, M., Zych, B.J., Steidel, C. C., & Chaffee, F. H. 2008, MNRAS, 385, 2011
Pettini, M., Madau, P., Bolte, M., et al. 2003, ApJ, 594, 695
Ryan-Weber, E. V., Pettini, M., & Madau, P. 2006, MNRAS, 371, L78
Ryan-Weber, E. V., Pettini, M., Madau, P., & Zych, B. J. 2009, MNRAS, 395, 1476
Scannapieco, E., Pichon, C., Aracil, B., et al. 2006, MNRAS, 365, 615
Schaye, J., Aguirre, A., Kim, T.-S., Rauch, M., & Sargent, W. L. W. 2003, ApJ, 596, 768
Shapley, A. E., Steidel, C. C., Pettini, M., Adelberger, K. L., & Erb, D. K. 2006, ApJ, 651, 688
Shull, J. M. 2014, ApJ, 784, 142
Shull, J. M., Roberts, D., Giroux, M. L., Penton, S. V., & Fardal, M. A. 1999, AJ, 118, 1450
Shull, J. M., Smith, B. D., & Danforth, C. W. 2012, ApJ, 759, 23
Shull, J. M., & van Steenberg, M. E. 1982, ApJS, 48, 92
Simcoe, R. 2006, ApJ, 653, 977
Simcoe, R. 2011, ApJ, 738, 159
Simcoe, R. M., Cooksey, K. L., Matejek, M., et al. 2011, ApJ, 743, 21
Songaila, A. 2001, ApJ, 561, L153
Songaila, A. 2005, AJ, 130, 1996
Smith, B. D., Hallman, E. J., Shull, J. M., & O'Shea, B. W. 2011, ApJ, 731, 6
Steidel, C. C., Adelberger, K. L., Giavalisco, M., Dickinson, M., & Pettini, M. 1999, ApJ, 519, 1
Stocke, J. T., Case, J., Donahue, M., Shull, J. M., & Snow, T. P. 1991, ApJ, 374, 72
Stocke, J. T., Keeney, B. A., Danforth, C. W., et al. 2013, ApJ, 763, 148
Tilton, E. M., Danforth, C. W., Shull, J. M., & Ross, T. L. 2012, ApJ, 759, 112
Tumlinson, J., Giroux, M.L., Shull, J. M., & Stocke, J. T. 1999, AJ, 118, 2148
Tumlinson, J., Thom, C., Werk, J. K., et al. 2011, Science, 334, 948
Tumlinson, J., Thom, C., Werk, J. K., et al. 2013, ApJ, 777, 59
Uson, J. M., Adams, J. J., Hill, G. J., & MacQueen, P. J. 2012, AAS Meeting 219, #312.01
Verner, D. A., Ferland, G. J., Korista, K. T., & Yakovlev, D. G.1996, ApJ, 465, 487
Vogel, S. N., Weymann, R. J., Rauch, M., & Hamilton, T. 1995, ApJ, 441, 162
Weisheit, J. 1974, ApJ, 190, 735
Werk, J. K., Prochaska, J. X., Tumlinson, J., et al. 2014, ApJ, 792, 8
Weymann, R. J., Vogel, S. N., Veilleux, S., & Epps, H. W. 2001, ApJ, 561, 559
Wolfe, A. M., Gawiser, E., & Prochaska, J. X. 2003, ApJ, 593, 235
Zhu, G., & Ménard, B. 2013, ApJ, 773, 16

TABLE 1
Absorption Line Data[a]

Ion	λ_0 (Å)	f	z-range $z_{\rm min} - z_{\rm max}$	$\log N_{\rm min}$[b] (N in cm^{-2})	τ_0[b]
C III	977.020	0.757	0.16 - 0.84	12.67	0.443
C IV	1548.204	0.176	0.00 - 0.16	12.87	0.176
N V	1238.821	0.116	0.00 - 0.45	13.15	0.116
O VI	1031.926	0.133	0.10 - 0.74	13.38	0.0819
Si III	1206.500	1.63	0.00 - 0.49	12.15	1.18
Si IV	1393.760	0.513	0.00 - 0.29	12.53	0.428

[a] Columns (1)–(4) list observed ion, rest wavelength (λ_0), and absorption oscillator strength (f) from Morton (2003), and redshift range observable between 1135-1796 Å in these primary transitions with the COS gratings (G130M and G160M).
[b] $N_{\rm min}$ is the minimum column density corresponding to the 30 mÅ equivalent width used as a lower cut-off for the survey. Possible line saturation is gauged by the optical depth at line center, $\tau_0 = (5.99 \times 10^{-4})(N_{13}\, f\lambda/b_{25})$, where N_{13} is the column density in units of 10^{13} cm^{-2}, λ is in Å, and b_{25} is the Doppler parameter in units of 25 km s^{-1}.

TABLE 2
Summary of Metal-Ion Densities[a]

Ion[a]	$N_{\rm abs}$[a]	Range in ($\log N$)[a] (N in cm^{-2})	$\Omega_{\rm ion}$(STIS)[a] (in $10^{-8}\ h_{70}^{-1}$)	$\Omega_{\rm ion}$(COS)[a] (in $10^{-8}\ h_{70}^{-1}$)
C III	77	12.67–14.19	$4.6^{+1.8}_{-0.8}$	$7.1^{+1.9}_{-1.2}$
C IV	49	12.87–14.87	$8.1^{+4.6}_{-1.7}$	$10.1^{+5.6}_{-2.4}$
N V	37	13.15–14.01	$0.9^{+1.3}_{-0.5}$	$1.9^{+0.6}_{-0.4}$
O VI	212	13.38–14.83	$33.9^{+9.3}_{-4.1}$	$38.6^{+4.8}_{-3.2}$
Si III	87	12.15–13.44	$1.1^{+0.8}_{-0.3}$	$1.4^{+0.3}_{-0.2}$
Si IV	31	12.53–13.94	$4.5^{+3.0}_{-1.2}$	$2.1^{+1.0}_{-0.5}$

[a] Columns (1)–(3) list observed ions, number of absorbers in COS survey in stated range of ion column densities ($\log N$). Minimum column density ($N_{\rm min}$) corresponds to 30 mÅ equivalent width in primary diagnostic line (Table 1). Maximum ($N_{\rm max}$) corresponds to last measured absorber at which survey statistics are reliable. Columns (4) and (5) list IGM mass density (at low z) of six ions, quoted as fractional contribution ($\Omega_{\rm ion} = \rho_{\rm ion}/\rho_{\rm cr}$) to closure density. These values are derived from HST/STIS survey (Tilton et al. 2012, revised as noted in text) and HST/COS survey (Danforth et al. 2014).

TABLE 3
Column-Density Distribution Fits[a]

Ion	C_0(weak)	β(weak)	C_0(strong)	β(strong)	$\log N_b$	$\log N_{\rm min}$	$\log N_{\rm max}$	$\Omega_{\rm ion}$[b] ($10^{-8}\, h_{70}^{-1}$)
C IV	2.7 ± 1.6	1.5 ± 0.2	1.6 ± 0.3	2.0 ± 0.2	13.546	12.87	15.0	10.2
Si IV	0.2 ± 0.1	1.8 ± 0.1	...	...	...	12.53	15.0	3.2
O VI	9.6 ± 0.9	1.6 ± 0.1	11 ± 2	3.9 ± 0.6	14.026	13.38	15.0	46.4
N V	0.4 ± 0.1	2.1 ± 0.2	...	...	...	13.15	15.0	3.5

[a] Power-law fits to the cumulative column density distribution, $d\mathcal{N}(>N)/dz$, of the form $C_0(N/N_0)^{-\beta}$, with fiducial column $N_0 = 10^{14}$ cm^{-2}. Ions Si IV and N V are fitted with a single power law, while C IV and O VI are fitted with a double power law (for weak and strong absorbers) matched at a break column density $\log N_b$.
[b] Value of ion density parameter, $\Omega_{\rm ion}$, integrating power-law distribution from $N_{\rm min}$ to $N_{\rm max}$, using Equations (A4), (A5), or (A6) in Appendix A.

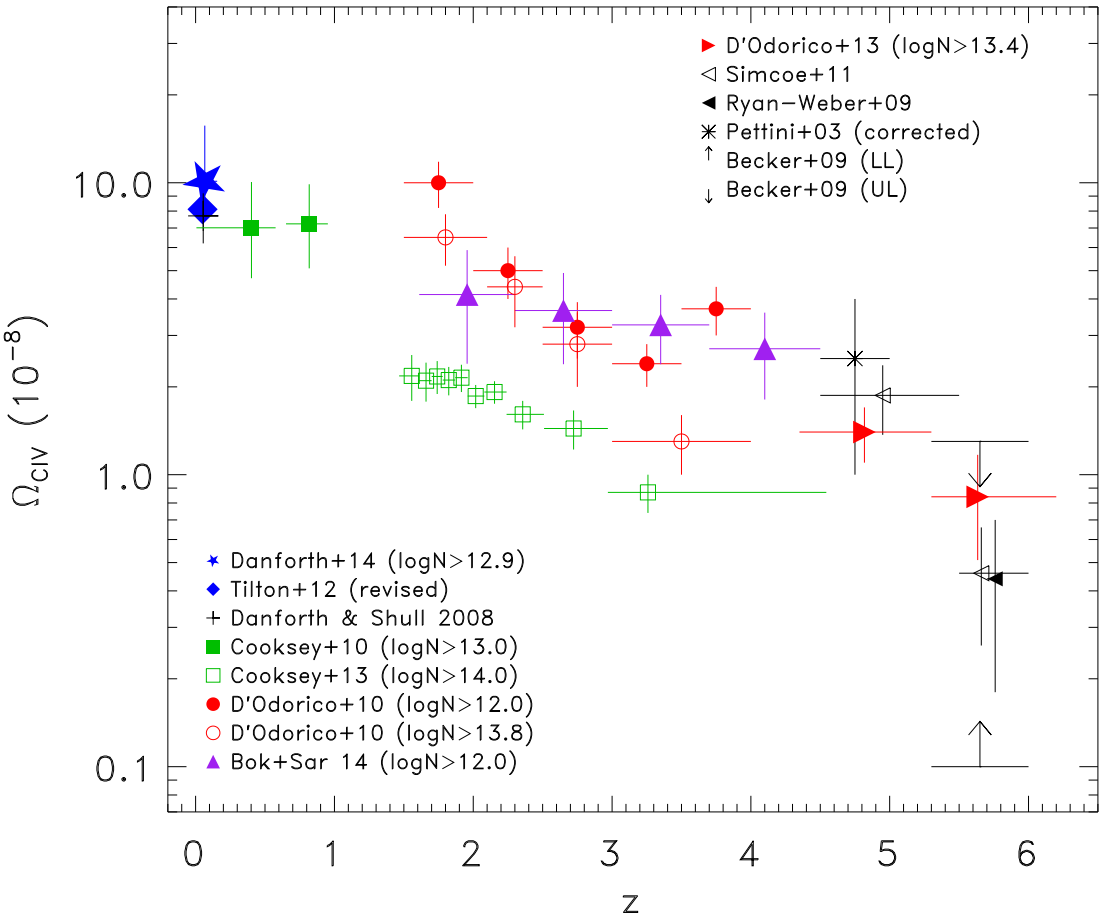

FIG. 1.— Redshift evolution of C IV mass density, with $\Omega_{\rm CIV}$ expressed relative to closure density in units of $10^{-8}\,h_{70}^{-1}$. Our HST/COS low-redshift measurement is shown together with values from past surveys. Lower envelope includes a survey at $1.5 < z < 4$ (Cooksey et al. 2013) that measures strong absorbers, while upper envelope includes weaker absorbers, with column densities in various ranges, from $13.4 < \log N_{\rm CIV} < 15$ (D'Odorico et al. 2013), from 12-15 (D'Odorico et al. 2010), 12.0-14.5 (Boksenberg et al. 2003), and 12.9-14.9 (Danforth et al. 2014). Taking into account corrections (see Appendix A) for these different N-ranges, the C IV abundance has evidently increased by a factor of 10 since $z \approx 5$.

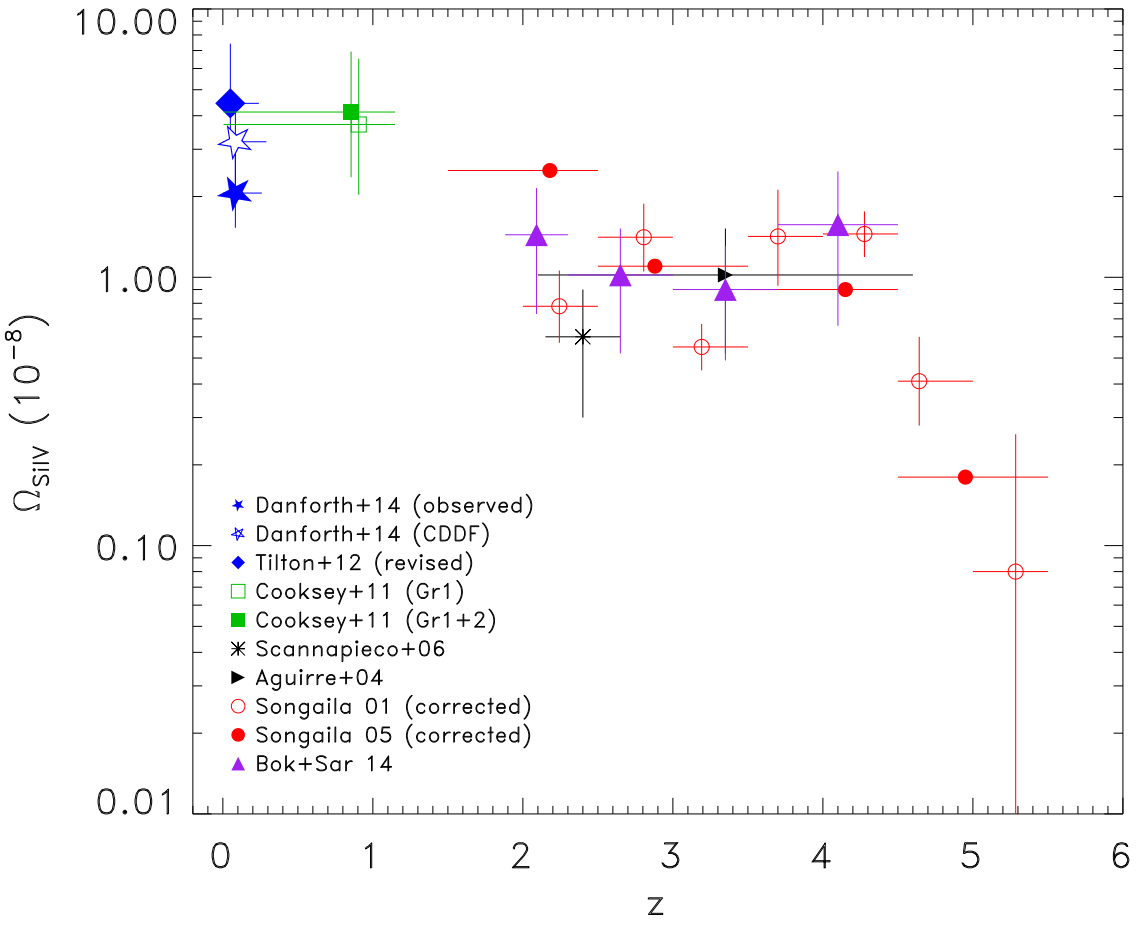

FIG. 2.— Redshift evolution of Si IV mass density, with $\Omega_{\rm SiIV}$ expressed relative to closure density in units of $10^{-8}\,h_{70}^{-1}$. Our HST/COS low-redshift measurement is shown together with values from past surveys with minimum column densities $\log N_{\rm SiIV}$ of 12.0 (Songaila 2001, 2005), 12.0 (Scannapieco et al. 2006), 12.0 (Boksenberg & Sargent 2014), and 12.5 (Danforth et al. 2014). The Si IV abundance has increased by over a factor of 10 since $z \approx 5$.

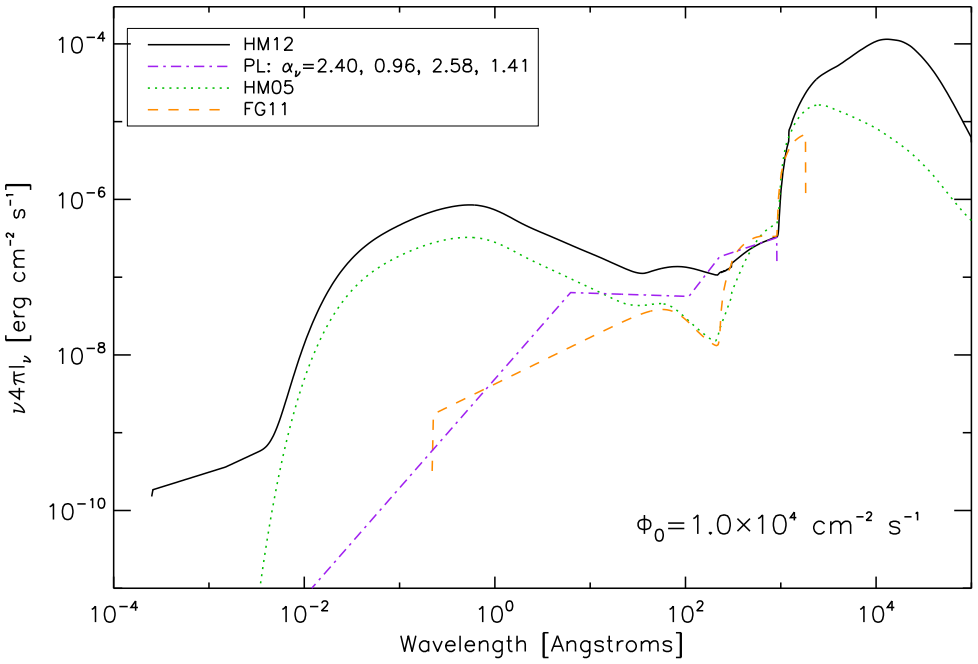

FIG. 3.— Several ionizing continua at $z = 0$ are explored in our analysis of ionization corrections. These spectral energy distributions (SED) plot the monochromatic flux, $\nu F_\nu \equiv 4\pi(\nu I_\nu)$ from HM12 (Haardt & Madau 2012), HM05 (unpublished 2005 tabulation from Haardt & Madau 2001), and FG11 (revised tabulation from Faucher-Giguère et al. 2009). The PL is a broken power-law SED that connects the $F_\nu \propto \nu^{-1.41}$ AGN composite EUV spectrum (Shull et al. 2012) to the soft X-ray (1 keV) spectrum of AGN in the Lockman Hole (Hasinger 1994). These SEDs are flux-normalized to common values $\Phi_0 = 1.0 \times 10^4$ phot cm^{-2} s^{-1}, the unidirectional, normally incident photon flux (see Appendix B).

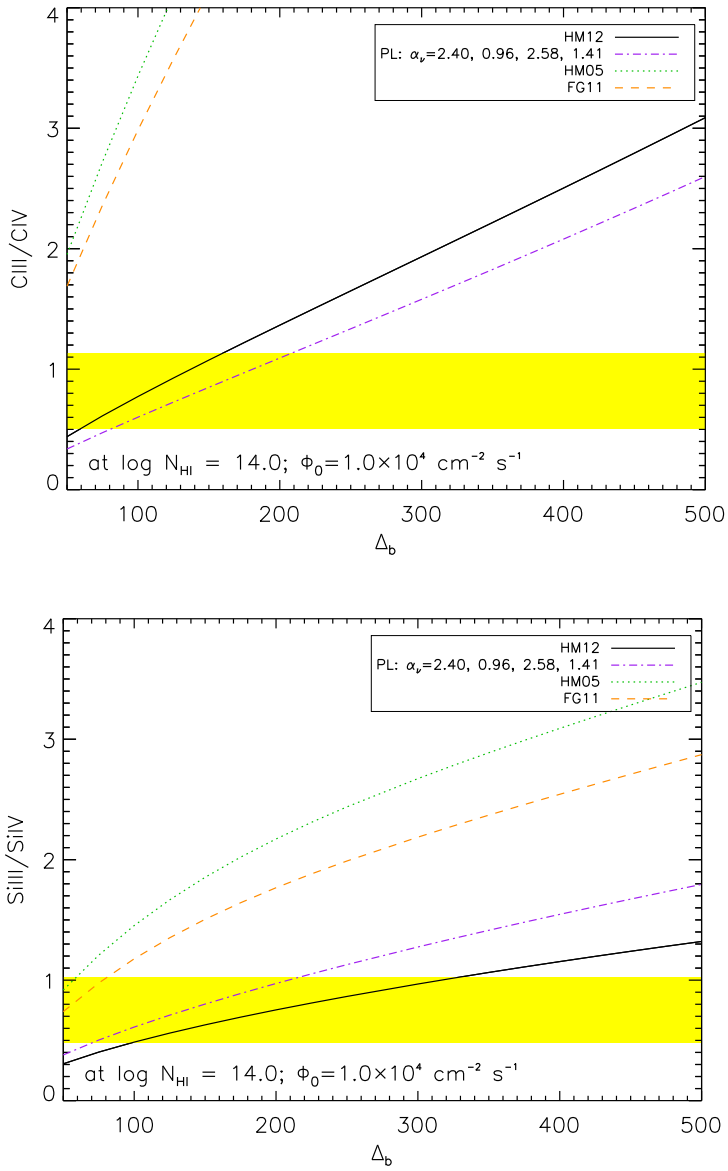

FIG. 4.— Mean ion abundance ratios, C III/C IV (top) and Si III/Si IV (bottom) for five ionizing SEDs, labeled in box. The top two curves (Haardt & Madau 2005; Faucher-Giguère et al. 2009) yield somewhat higher ratios than observed (yellow bands), while the three lower curves (Haardt & Madau et al. 2012, and broken power law PL) give ratios consistent with our low-redshift COS observations, $\Omega_{\rm CIII}/\Omega_{\rm CIV} = 0.70^{+0.43}_{-0.20}$ and $\Omega_{\rm SiIII}/\Omega_{\rm SiIV} = 0.67^{+0.35}_{-0.19}$.

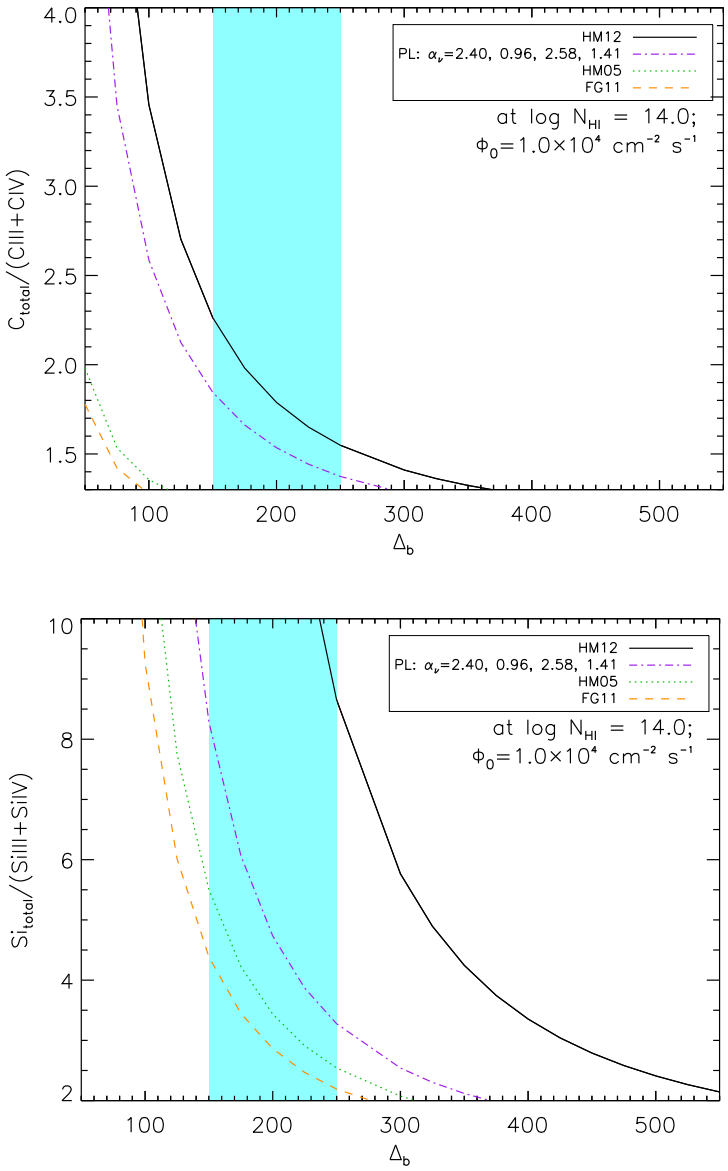

FIG. 5.— Ionization correction factors for total carbon and silicon relative to the two observed ion states, (C III + C IV) and (Si III + Si IV), vs. baryon overdensity Δ_b . Curves correspond to ionizing continua labeled in boxes and plotted in Figure 3. Vertical (blue) band shows the range of $\Delta_b = 200 \pm 50$ that provides consistent ionization corrections and metallicities for Si and C, with enhanced Si/C. See further discussion in Section 3.2.

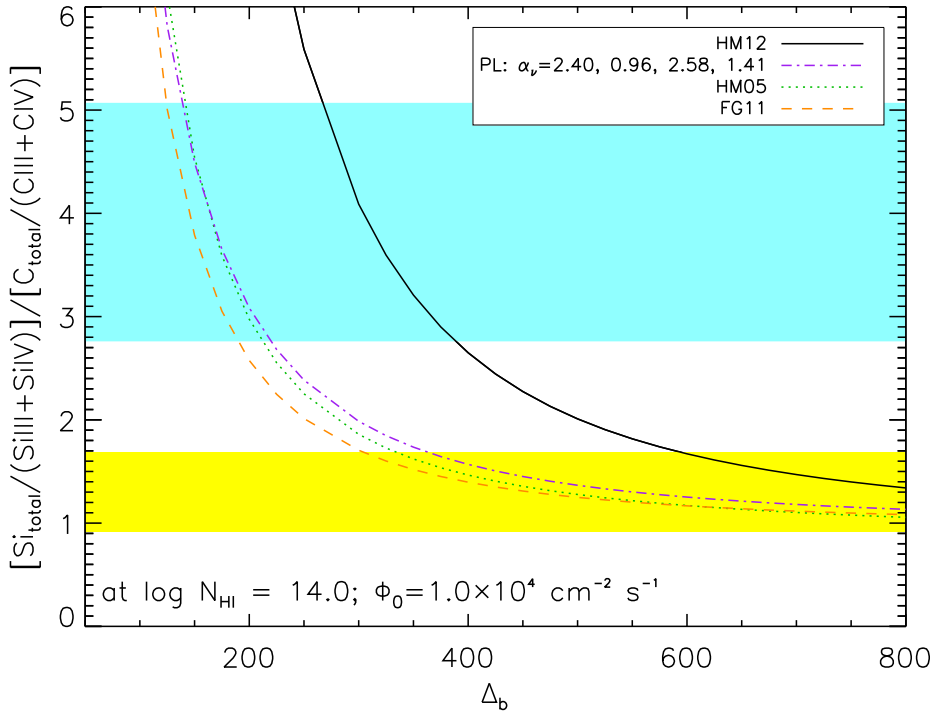

FIG. 6.— Ratio of the Si and C ionization correction factors, CF_{Si}/CF_C, plotted vs. baryon overdensity Δ_b for several SEDs labeled in box. Self-consistency requires that the inferred metallicities agree with the Si/C mass-density ratio, which is 0.238 for solar abundances or 3× higher for alpha-enhanced Si/C. This condition requires a ratio, $CF_{Si}/CF_C = (1.17^{+0.52}_{-0.25})\,[(\rho_{Si}/\rho_C)/0.238]$, shown for Si/C in solar ratio (bottom band in yellow) and enhanced by factor of 3 (top band in blue).

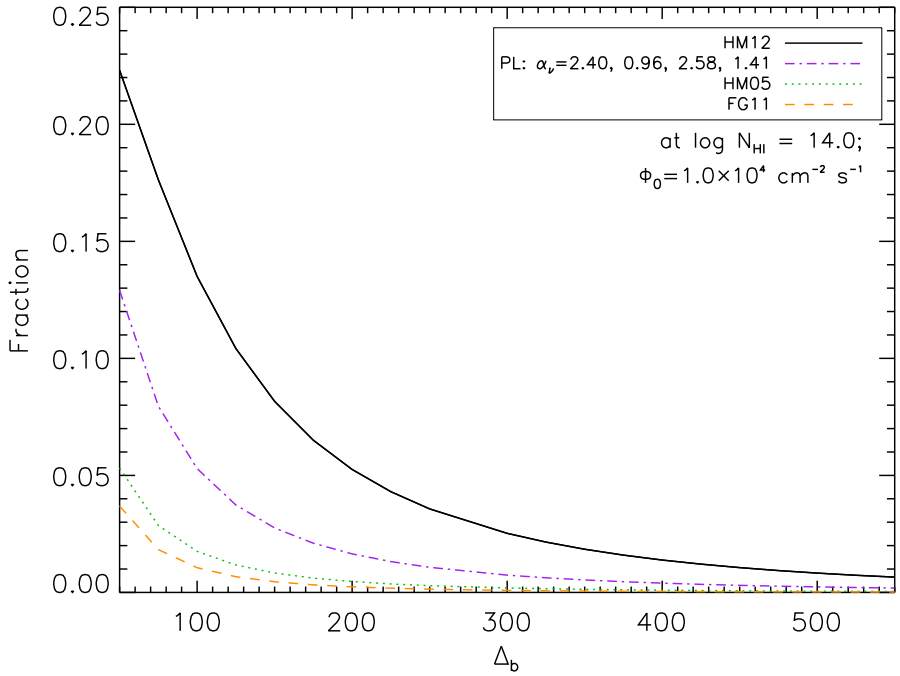

FIG. 7.— Ionization fraction of O VI vs. baryon overdensity Δ_b, for several metagalactic radiation fields. The top two curves show fraction for the full HM12 (Haardt & Madau 2012) background, and removing photons above the carbon K-edge ($E \geq 290$ eV). The three lower curves assume other backgrounds: PL (broken power law); HM05 (Haardt & Madau 2001); FG11 (Faucher-Giguère et al. 2009). In the latter three cases, the photoionized O VI fraction is small at $\Delta_b \approx 200 \pm 50$.